Knockout of HD domain 5'-nucleotidase in *T. brucei* triggers cell death linked to DNA damage and downregulation of glutamine uptake

Yue Wen Deng[1], Michael A. Pontikos[1], Hamid Baniasadi[1], Noelle S. Williams[1], Margaret A. Phillips[1,2*]

Departments of Biochemistry[1], and Pharmacology[2], University of Texas Southwestern Medical Center, Dallas, Texas, United States of America

Short title: 5'-HDNT in Trypanosoma brucei pyrimidine metabolism

*Corresponding author: margaret.phillips@utsouthwestern.edu (MAPh)

Abstract

African trypanosomiasis is a fatal vector-borne disease caused by the protozoal parasite *Trypanosoma brucei*. This parasite encodes both *de novo* and salvage pathways for pyrimidine nucleotide biosynthesis, but in contrast to other eukaryotes, it lacks a dedicated enzyme to interconvert between cytidine (C) and uridine (U) nucleotide pools. Instead, we previously reported that nucleotide interconversion was mediated by thymidine kinase (TK) and an unknown 5'-nucleotidase enzyme. *T. brucei* encodes multiple potential 5'-nucelotidases, including one from the histidine-aspartate (HD) family (5'-HDNT) and two from the haloacid dehalogenase (HAD1 and HAD2) superfamily of metalloenzymes, but their relative roles and function in nucleotide metabolism remained unexplored. Herein we report that enzymes from both families catalyze dephosphorylation of pyrimidine monophosphate nucleotides, but only 5'-HDNT exhibited high activity on dCMP and was essential for *T. brucei* growth, while HAD1 and HAD2 were dispensable. Growth arrest upon loss of 5'-HDNT expression was rescued by ectopic expression of human dCMP deaminase (*Hs*DCTD), which creates an alternate route for conversion between C and U pools. Knockout of 5'-HDNT led to depletion of pyrimidine pathway metabolites, altered ratios of pyrimidine to purine nucleotides, and DNA damage. Surprisingly, intracellular glutamine, the precursor of *de novo* pyrimidine biosynthesis, was also significantly reduced, and isotope tracing assays identified a deficiency in glutamine uptake, suggesting that the glutamine transporter was downregulated in response to loss of 5'-HDNT. This response would likely exacerbate perturbation of pyrimidine pathway homeostasis, suggesting we have uncovered a potential regulated cell death pathway in *T. brucei*.

Author Summary

Trypanosome parasites cause fatal neurologic disease if untreated, and over 50 million people in tropical and subtropical countries are at risk for contracting the disease. Current treatments suffer from toxic side effects or involve complicated therapies. Further understanding of trypanosome biology is necessary to inform new drug development efforts. Here we show that the pyrimidine biosynthesis pathway contains 5'-nucleotidases that facilitate recycling between monophosphate nucleotide and nucleoside pools, and this interconversion is essential to parasite survival. Cells lacking 5'-HDNT experience nucleotide imbalance and DNA strand breaks. Rather than increasing nutrient uptake to repair the damage, we observe downregulation of glutamine uptake and subsequent cell death. This unexpected result points to an unexplored parasite stress response pathway that could be exploited for development of new therapies.

47 **Introduction**

48

49 The protozoal parasite *Trypanosoma brucei* causes the disease human African trypanosomiasis
50 (HAT), also called sleeping sickness. *T. brucei* is transmitted to the mammalian host by the bite of
51 a tsetse fly (*Glossina*) and replicates in the blood before crossing the blood brain barrier, leading
52 to progressive neurologic disease that is fatal if untreated [1]. While recent efforts by the World
53 Health Organization have reduced disease incidence, the geographical distribution of the tsetse fly
54 vector places around 55 million people at risk [2, 3]. In addition, livestock infection by *T. brucei*
55 causes animal trypanosomiasis (nagana), leading to protein malnutrition, and the substantial
56 animal reservoir represents an additional challenge to disease eradication [4, 5]. Current therapies
57 for HAT have toxic side effects or require intravenous administration, which complicates treatment
58 in rural areas [6]. New drugs are necessary to address both animal and human disease.

59

60 Maintenance of adequate and balanced dNTP pools is essential for cell proliferation and survival,
61 as well as accurate genomic replication and repair [7]. Pyrimidine biosynthesis in *T. brucei* relies
62 on both *de novo* and salvage pathways to generate the precursors for DNA, RNA, nucleotide sugars,
63 and phospholipids (Fig 1) [8, 9]. *De novo* pyrimidine synthesis depends on glutamine, while
64 nucleoside salvage occurs mainly through uracil [8]. Despite the term "salvage," enzymes in the
65 salvage pathway also have essential functions in the *de novo* pyrimidine biosynthetic pathway.
66 Thymidine kinase (TK), initially believed to be redundant given the existence of the *de novo*
67 pathway, was found by us and others to be critical for maintaining dUMP pools [10, 11]. We found
68 that while loss of TK was lethal, human dCMP deaminase (*Hs*DCTD) rescued TK knockout cells
69 by providing an alternate route for dUMP formation [10]. Metabolite analysis showed that loss of

70 TK led to dTTP depletion and accumulation of dThd, dCtd, and dUrd nucleosides, and this finding
71 led to our discovery of previously unannotated 5'-nucleotidases that convert deoxypyrimidine
72 monophosphate nucleotides into nucleosides. Hence, the mechanism of cell death in TK knockout
73 cells occurs through unopposed 5'-nucleotidase activity that creates a dead-end buildup of
74 nucleoside products, thereby sequestering resources away from nucleotide synthesis [10].
75
76 Our previous work identified several potential 5'-nucleotidase genes through bioinformatic
77 analysis of the *T. brucei* genome, including several from the metal-dependent protein phosphatase
78 (PPM) family, haloacid dehalogenase (HAD) superfamily, and one from the histidine-aspartate
79 (HD) domain family [10]. Among these candidates, three genes were identified to contain PFAM
80 domains [12] annotated to have 5'-nucleotidase activity: HD domain 5'-nucleotidase
81 (Tb927.9.10830) (5'-HDNT), HAD phosphatase (Tb927.8.7510) (HAD1), and HAD hydrolase
82 (Tb927.9.10500) (HAD2). We showed that the *T. brucei* 5'-HDNT is a homolog of YfbR from *E.*
83 *coli* and catalyzed dephosphorylation of a range of deoxyribonucleotide monophosphates (dNMPs)
84 using cobalt as a metal cofactor, but it was more promiscuous than the bacterial enzyme in its
85 reactivity towards ribonucleotide monophosphate substrates (NMPs) [10, 13]. *T. brucei* 5'-HDNT
86 was most active towards dUMP, dTMP, and dCMP substrates, and dUMP and dTMP are the
87 products of TK. The existence of multiple genes predicted to catalyze 5'-nucleotidase activity in
88 *T. brucei* suggested that more than one may potentially contribute to cell death in TK-deficient
89 cells. Furthermore, our preliminary analysis did not address the relative contributions of 5'-HDNT
90 or the HAD family putative phosphatases/hydrolases HAD1 and HAD2 to *T. brucei* pyrimidine
91 metabolism and parasite biology.
92

93 Herein we describe a comprehensive characterization of the above three *T. brucei* HD and HAD
94 family enzymes identified by our bioinformatic analysis. We conducted kinetic characterization of
95 the recombinant enzymes to explore their substrate specificity, and we evaluated their essentiality
96 to blood form *T. brucei* by the generation of null or conditional null (c-null) cell lines. We found
97 that 5'-HDNT is an essential enzyme that prefers pyrimidine dNMPs as substrates and was the
98 only one of the three characterized enzymes to have high efficiency on dCMP. In contrast, neither
99 HAD1 nor HAD2 were essential. Both HAD1 and HAD2 demonstrated phosphatase activity on
100 dNMP and NMP substrates, but only HAD2 showed high activity as a 5'-nucleotidase, while
101 HAD1 preferred triphosphate nucleotide substrates to the monophosphate nucleotides.
102 Surprisingly, depletion of 5'-HDNT after conditional knockout of the gene led to L-glutamine (L-
103 Gln) deficiency, which was accompanied by depletion of *de novo* pathway pyrimidine metabolites,
104 nucleotide sugars, and phospholipid precursors. Finally, quantitative analysis of dNTP pools
105 showed reduced levels of both dTTP and dCTP, leading to imbalanced dNTP ratios and to DNA
106 strand breaks and DNA damage. We propose a model whereby the observed nucleotide imbalance
107 leads to DNA damage that then leads to the downregulation of L-Gln uptake and to cell death.
108 Together, our data reveal an unexpected metabolic response to disruption of pyrimidine nucleotide
109 balance and a key role of 5'-HDNT in maintaining this balance.
110

111 **Results**

112

113 ***T. brucei* encodes multiple nucleotidases with differing substrate specificities**

114 To study the activity and substrate preferences of potential 5'-nucleotidases in the *T. brucei*
115 genome, we recombinantly expressed and purified the proteins encoded by three genes: 5'-HDNT
116 (Tb927.9.10830), HAD1 (Tb927.8.7510), and HAD2 (Tb927.9.10500). Attempts to purify full-
117 length HAD2 were unsuccessful as the protein formed inclusion bodies and was insoluble. To
118 overcome this issue, we generated an N-terminal truncation construct (HAD2_Δ1-136). The
119 truncation site was selected based on alignment of HAD protein sequences from seven other
120 organisms with *T. brucei* HAD2 (S1 Fig). The truncation removed an amino acid sequence that
121 was found only in kinetoplastid homologs, and thus we reasoned that the enzymatic domain of
122 HAD2 started after amino acid 136, corresponding to the approximate start site from other species.
123 Truncated HAD2_Δ1-136 expressed to high levels and was used for all kinetic analyses.

124

125 We analyzed the steady-state kinetics of each enzyme using a colorimetric endpoint assay that
126 measures the production of inorganic phosphate (P_i). Previously, we reported the specific activity
127 of 5'-HDNT but had not determined steady-state kinetic constants [10]. All three enzymes
128 catalyzed the metal-dependent formation of phosphate. 5'-HDNT was most active in the presence
129 of Co^{2+} while HAD1 and HAD2 preferred Mg^{2+} (Fig 2A-2C). 5'-HDNT also showed activity in
130 the presence of Mg^{2+}, but it was 7-fold lower than for Co^{2+} while HAD1 and HAD2 showed a
131 similar reduction in activity with Co^{2+} or Mn^{2+} compared to Mg^{2+}. 5'-HDNT and HAD2 both
132 showed selective 5'-nucleotidase activity, catalyzing the dephosphorylation of a range of purine
133 and pyrimidine dNMPs and NMPs. Similar to our previous report [10], 5'-HDNT had broad

134 substrate specificity, but it showed a clear preference for pyrimidine dNMPs with k_{cat}/K_M values
135 that were 5-10-fold higher on dNMPs (dCMP, dUMP, and dTMP) than for purine nucleotides
136 (dAMP and dGMP), while it was 20-60-fold less active on the corresponding NMPs (Fig 2D and
137 S1A Table). In comparison, HAD2 showed a narrow substrate preference, preferring dTMP by 6-
138 fold over dAMP and by 10-20-fold over all other dNMP and NMP substrates (Fig 2F and S1C
139 Table). For both 5'-HDNT and HAD2, the preferred substrates were distinguished by having lower
140 K_M values (μM vs mM) than observed for less favored substrates. Of note, 5'-HDNT was the only
141 enzyme of the three tested to show high catalytic efficiency towards dCMP, with a K_M that was 5-
142 and 20-fold lower than those for HAD2 and HAD1, respectively.
143
144 HAD1 showed significantly lower activity as a 5'-nucleotidase than 5'-HDNT or HAD2, with K_M
145 values in the high millimolar range for all dNMP or NMP substrates (Fig 2E and S1B Table). It
146 showed the highest efficiency towards dUMP, but the k_{cat}/K_M towards this substrate was 6-20-fold
147 lower than observed for 5'-HDNT or HAD2 on their preferred substrates (dCMP and dTMP
148 respectively). To probe whether HAD1 catalyzed a different reaction, we tested its activity on a
149 range of dNTP and NTP substrates. We found that it catalyzed phosphate formation from the
150 preferred trinucleotide substrates (CTP, dCTP, and GTP) with a k_{cat}/K_M that was 10-100-fold
151 higher than observed for any of the monophosphate substrates (S1B Table), while it had no activity
152 on purine or pyrimidine deoxyribonucleotide or ribonucleotide diphosphates (data not shown). As
153 our assay followed the production of phosphate, it is unclear whether HAD1 catalyzes removal of
154 a single phosphate from the trinucleotide substrates to generate dinucleotide phosphates, or if it
155 can catalyze formation of the nucleoside sequentially (as described for plant R-proteins [14]), or
156 if it might function to transfer phosphate to another dinucleotide if given a donor dNDP instead of

157 water (e.g. nucleoside-diphosphate kinase activity). Given that HAD1 was not essential (below),
158 we did not pursue these questions and focused instead on 5'-HDNT.
159
160 **5'-HDNT is essential in bloodstream form *T. brucei* while HAD1 and HAD2 are dispensable**
161 We investigated the essentiality of 5'-HDNT, HAD1, and HAD2 in bloodstream form *T. brucei*
162 by gene knockout via homologous recombination in single marker (SM) cells. Since *T. brucei* is
163 diploid, two rounds of recombination were performed to replace both alleles with antibiotic
164 resistance markers. Using this method, null cell lines of HAD1 and HAD2 were generated showing
165 that neither enzyme is essential (S2A Fig, S2B Fig, S2D Fig, and S2E Fig). However, attempts to
166 generate a null 5'-HDNT cell line were unsuccessful, suggesting it was essential. To further study
167 the role of 5'-HDNT on growth and parasite metabolism, we generated a conditional knockout cell
168 line (c-null) by introducing a tetracycline (Tet)-regulated FLAG-tagged *T. brucei* 5'-HDNT
169 expression construct before knockout of the second 5'-HDNT allele, creating the 5'-HDNT$^{-/-}$
170 Tet(5'-HDNT) cell line (S2 Table). Growth arrest of these cells occurred by 48 h after Tet removal
171 in media containing either normal or dialyzed FBS, indicating essentiality (Fig 3A, Fig 3D, and
172 S3 Fig). 5'-HDNT mRNA transcript and protein levels were depleted by 24 h after Tet removal,
173 indicating appropriate Tet regulation of the rescue construct (Fig 3B, Fig 3C, and S4A Fig). The
174 observed growth arrest could not be rescued by supplementation of the media with various
175 pyrimidine nucleosides and bases, showing they were unable to restore normal balance of the
176 metabolic cycle (S5 Fig).
177

178 **Human dCMP deaminase rescues 5'-HDNT knockout**

179 Unlike other eukaryotes, *T. brucei* lacks a route for direct conversion of dCMP to dUMP and thus
180 has no direct pathway to allow for exchange between these pyrimidine pools [10]. In mammals,
181 this reaction is performed by dCMP deaminase (DCTD). Given that 5'-HDNT catalyzes the
182 conversion between dCMP and its nucleoside dCtd, which can then be used to make dUMP, we
183 tested whether introducing *Hs*DCTD into 5'-HDNT c-null cells could restore parasite viability,
184 similarly to our previous observation for the TK null cell line [10]. We generated a 5'-HDNT null
185 cell line that expressed Tet-regulated FLAG-tagged *Hs*DCTD in place of the regulated copy of 5'-
186 HDNT (5'-HDNT$^{-/-}$Tet(*Hs*DCTD)) (S2 Table). In the presence of Tet we confirmed expression of
187 both *Hs*DCTD mRNA transcript and FLAG-tagged *Hs*DCTD and observed that cell growth rates
188 were similar to the c-null line expressing ectopic *T. brucei* 5'-HDNT (Fig 3A, Fig 3D-3F, and S4B
189 Fig). Removal of Tet resulted in a growth defect in both normal and dialyzed FBS containing
190 media, with a more severe phenotype observed in dialyzed media (Fig 3D). The ability of *Hs*DCTD
191 to restore growth in 5'-HDNT knockout cells suggests 5'-HDNT functions together with TK as
192 part of an essential metabolic cycle that allows for interconversion between pyrimidine nucleotide
193 pools in *T. brucei*.

194

195 **De novo pyrimidine synthesis pathway metabolites are depleted upon 5'-HDNT knockout**

196 To determine the metabolite profile of cells lacking 5'-HDNT, we analyzed 5'-HDNT$^{-/-}$Tet(5'-
197 HDNT) cells by liquid chromatography with tandem mass spectrometry (LC-MS/MS). Cells were
198 collected for analysis after growth for 48 h ±Tet in media with normal serum. We found that
199 metabolites in the *de novo* pyrimidine synthesis pathway were the most significantly impacted
200 upon loss of 5'-HDNT expression (-Tet), with L-Gln, carbamoyl phosphate, and UMP each

201 exhibiting a 3-5-fold reduction (Fig 4A, S6A Fig, S6B Fig, S6C Fig and S3 Table). Other
202 significantly depleted metabolites included CDP-choline (4-fold decrease), CDP-ethanolamine (4-
203 fold decrease), UDP-glucose (4-fold decrease), and UDP-GlcNAc (3-fold decrease). In contrast,
204 pyrimidine nucleosides and monophosphate nucleotides were not significantly changed (S7A Fig
205 and S4 Table). As an orthogonal method, we used a fluorescence-based PCR assay to quantify
206 nucleotide levels in these cells and found that dTTP and dCTP levels were reduced 30-50%
207 respectively after Tet removal (Fig 5A and S5 Table). Purine nucleotides were unchanged ±Tet.
208 The ratio of the four deoxynucleotides dTTP:dATP:dCTP:dGTP was 5:3:1:1 in the +Tet condition
209 and changed to 3:3:0.5:1 upon removal of 5'-HDNT. The largest differences were observed for
210 dCTP, with the dCTP:dGTP ratio decreased by 3-fold and the dATP:dCTP ratio increased ~2-fold
211 (Fig 5B). The dTTP:dGTP ratio decreased by 2-fold while the dTTP:dATP ratio decreased by 30%.
212

213 We also performed metabolomic analysis on the 5'-HDNT$^{-/-}$Tet(*Hs*DCTD) cells after growth for
214 48 h ±Tet in normal serum media. The metabolite profile was essentially identical to that of 5'-
215 HDNT$^{-/-}$Tet(5'-HDNT) cells, with significant depletion of L-Gln, carbamoyl phosphate, and UMP
216 observed (Fig 4B, S6D Fig, S6E Fig, S6F Fig, S7B Fig, and S3 Table). Two metabolites that
217 appeared in the *Hs*DCTD rescue cell line but not in the 5'-HDNT rescued c-null line were dCMP,
218 which had a 3-5-fold increase, and dUMP, which exhibited a 2.5-fold decrease. This pattern of
219 metabolites reflects an apparent dependence of these cells on the enzymatic activity of *Hs*DCTD
220 for formation of dUMP since we observe substrate build-up and product loss upon downregulation
221 of *Hs*DCTD expression. No significant metabolite changes were observed in the HAD1 and HAD2
222 knockout cell lines (S2C Fig, S2F Fig, and S6 Table). These results reveal an unexpected depletion

223 of *de novo* pathway intermediates upon 5'-HDNT knockout accompanied by reduced pyrimidine
224 dNTP pools relative to purine dNTP pools.
225
226 **Thymidine kinase and 5'-HDNT activity are necessary for parasite survival**
227 TK and 5'-HDNT catalyze opposing enzymatic reactions in *T. brucei* (Fig 1). In our previous
228 studies we found that loss of TK led to depletion of pyrimidine nucleotide pools caused by the
229 unopposed dephosphorylation of these metabolites by cellular 5'-nucleotidases. Rescue of both 5'-
230 HDNT and TK knockout by expression of *Hs*DCTD suggests that this pathway plays a role in
231 pyrimidine interconversion, and that the cells require the ability to cycle between phosphorylated
232 and unphosphorylated pyrimidine nucleotides/nucleosides. However, the loss of cell viability
233 might be due to the unopposed activity of TK or 5'-HDNT in the absence of the other, suggesting
234 the possibility that deletion of both activities may restore cell viability. To test this hypothesis, we
235 generated a double knockout of *T. brucei* TK and 5'-HDNT by sequentially creating conditional
236 knockouts of each gene, with retrieval of resistance markers using Cre recombinase between each
237 set. This method was used due to the limited number of available antibiotic resistance markers.
238 The successful replacement of all four alleles was confirmed by PCR (S8A Fig). The resulting
239 TK/5'-HDNT double conditional knockout contains two regulated constructs, with both *Tb*TK and
240 *Tb*5'HDNT expression under Tet control (S2 Table). Removal of Tet caused a concurrent decrease
241 in both TK and 5'-HDNT mRNA as shown by qPCR (Fig 6B) and protein levels as shown by a
242 capillary electrophoresis-based Western blot assay (Fig 6C and S4C Fig). The TK/5'-HDNT c-
243 null cells showed growth arrest within 24-48 h in normal and dialyzed media and exhibited rapid
244 parasite death in both media conditions by 72 h after Tet removal (Fig 6A). Analysis of metabolite
245 levels upon Tet removal (S8B Fig) showed depletion of dTTP and its precursors dTDP and dTMP,

246 as well as UDP-sugars and CDP-choline (Fig 6D, Fig 6E, and S7 Table). Monophosphate
247 nucleotides dCMP and dUMP were slightly increased. L-Gln levels were not significantly changed,
248 suggesting the mechanism of cell death differs compared to the 5'-HDNT knockout alone. The
249 impact on the metabolite pools of the TK/5'-HDNT double knockout was similar to that observed
250 in TK null cells [10] and suggests that other nucleotidases beyond 5'-HDNT are able to catalyze
251 dephosphorylation of the deoxypyrimidine mononucleotides. Consistently, HAD2 nucleotidase
252 has a strong substrate preference for dTMP and a similar k_{cat}/K_M to 5'-HDNT on both dTMP and
253 dUMP (Fig 2F). Thus, whether cells could survive without TK if all monophosphate 5'-
254 nucleotidase activity were fully removed remains an open question. However, the finding that only
255 5'-HDNT shows high reactivity towards dCMP, taken together with the rescue of both TK and 5'-
256 HDNT knockouts by *Hs*DCTD, suggests that recycling from C pools back to T and U pools is an
257 essential cellular function.
258

259 **L-Gln uptake is impaired in 5'-HDNT knockout cells**

260 The standard *T. brucei* growth media used for these studies contains 4 mM L-Gln; thus, the
261 observed reduction in intracellular L-Gln levels upon loss of 5'-HDNT expression suggested the
262 possibility of a transport defect. To address this possibility, the ability of 5'-HDNT$^{-/-}$Tet(5'-HDNT)
263 cells to take in $^{13}C_5{}^{15}N_2$-L-Gln was assessed using an oil spin method to separate free label from
264 cells [15]. 5'-HDNT$^{-/-}$Tet(5'-HDNT) cells were grown ±Tet for 48 h (Fig 7A) and then monitored
265 for $^{13}C_5{}^{15}N_2$-L-Gln uptake over 20 second increments for a total of 2 minutes. SM wild-type cells
266 were also studied as a control. Cells lacking 5'-HDNT (-Tet) were deficient in L-Gln uptake
267 compared to wild-type cells or cells expressing ectopic 5'-HDNT (+Tet), with ~10-fold less
268 labeled L-Gln measured in cells across the time course (Fig 7B, S9A Fig, and S10 Fig). $^{13}C_5{}^{15}N_2$-

269 L-Gln was traced into downstream metabolites glutamate, succinate, and UMP (Fig 7C, Fig 7D,
270 and S9B-D Fig), and these metabolites were found to exhibit a similar pattern of decreased heavy
271 atom labeling, confirming the L-Gln uptake deficiency by reduced incorporation into these
272 metabolites. To show that cells lacking 5'-HDNT (-Tet) were still competent to transport amino
273 acids, $^{13}C_5$-L-ornithine uptake was measured as a control in comparison to cells expressing 5'-
274 HDNT (+Tet) and SM wild-type cells. Uptake of $^{13}C_5$-L-ornithine was similar in all three
275 conditions, showing that the L-Gln transport deficiency was not due to loss of cell viability or
276 transport capability (Fig 7E).
277

278 **PCR-based measurement of DNA damage in 5'-HDNT knockout cells**

279 Fidelity of DNA synthesis has been shown to be dependent on balanced nucleotide pools in
280 mammalian and yeast cells [16-21]. Given the change in pyrimidine nucleotide levels and overall
281 nucleotide ratios observed upon 5'-HDNT knockout, we investigated whether 5'-HDNT$^{-/-}$Tet(5'-
282 HDNT) cells had evidence of DNA damage using a published PCR-based technique [22, 23]. Cells
283 were grown in normal media ±Tet for 24, 36, or 48 h and lesion density was assessed on a 10-kb
284 fragment of genomic DNA. The number of DNA lesions within the 10-kb fragment increased from
285 0.08 to 1.1 over the time course after Tet removal (Fig 8A). As a control, cells were treated with
286 known DNA damaging agents hydroxyurea (HU) (100 μM) and methyl methanesulfonate (MMS)
287 (0.002%) for 24 h, with these treatments generating 0.5-0.8 lesions in this assay (Fig 8A). Cell
288 growth over 48 h was measured as a control, showing the expected reduction after Tet removal for
289 the 5'-HDNT$^{-/-}$Tet(5'-HDNT) cells (Fig 8B). Both control DNA damaging agents also reduced the
290 cell growth rate (Fig 8B). To control for the potential influence of generalized cell death as a cause
291 of DNA damage, we treated cells with trypanocidal and trypanostatic agents at a range of

292 concentrations relative to their published EC_{50} values (0.5 – 2x) and observed the expected effects
293 on growth with increasing concentrations of compounds (Fig 8D). Despite similar growth defects
294 to the 5'-HDNT knockout, impact on polymerase-blocking lesions was varied, with eflornithine
295 causing 0.7-1.0 lesions / 10kb and pentamidine causing 0.8-1.3 lesions / 10kb (Fig 8C). In contrast,
296 suramin and fexinidazole treatment did not produce DNA damage lesions despite both causing
297 strong growth defects (Fig 8C). These results are consistent with the mechanisms of action for
298 eflornithine and pentamidine. Eflornithine is a suicide inhibitor of ornithine decarboxylase, the
299 first committed step in *T. brucei* polyamine biosynthesis [24]. Polyamines have been shown to
300 bind DNA, facilitating chromatin compaction and DNA charge stabilization [25]. While the
301 mechanism of action is unknown, pentamidine treatment has been implicated in loss of kinetoplast
302 DNA in *T. brucei* [26].
303

304 **DNA alkaline comet assay to evaluate DNA damage in 5'-HDNT knockout cells**

305 As an alternative approach, we performed an alkaline comet assay to evaluate DNA strand breaks.
306 5'-HDNT$^{-/-}$Tet(5'-HDNT) cells were grown for 48 h ±Tet, and we confirmed depletion of mRNA
307 and protein levels 48 h after Tet removal (Fig 9C, Fig 9D, and S4D Fig). As a positive control, SM
308 wild-type cells and 5'-HDNT$^{-/-}$Tet(5'-HDNT) cells were treated with MMS (0.002%) for 24 h
309 prior to the assay. Comet tails were visible in 5'-HDNT knockout cells (Fig 9A), indicating
310 migration of DNA fragments proportional to the amount of DNA damage. In addition, those cells
311 had significantly more DNA strand breaks as measured by tail moment, a parameter that combines
312 tail length with the percentage of cellular DNA found in the tail [27]. The mean tail moment
313 increased from 20 to 50 between the +Tet and -Tet conditions, similar to the effect of MMS on

314 +Tet and wild-type SM cells (Fig 9B and S11 Fig). Together, these data support the hypothesis

315 that cells lacking 5'-HDNT accumulate unrepaired DNA strand breaks.

316 **Discussion**

317

318 *T. brucei* encodes both *de novo* and salvage pathway enzymes for production of essential
319 pyrimidine nucleotides. We previously found that TK, while annotated as a salvage enzyme, also
320 played an unexpected and essential role in *de novo* pyrimidine biosynthesis and was required to
321 ensure sufficient dUMP, dTMP and dCMP pools for the synthesis of pyrimidine dNTPs [10]. In
322 the absence of TK, the unopposed back reaction catalyzed by 5'-nucleotidases caused depletion of
323 dTTP and cell death. Herein we describe the characterization of three enzymes with 5'-
324 nucleotidase activity (5'-HDNT, HAD1, and HAD2) in *T. brucei*, including their role in
325 maintaining balanced pyrimidine dNTP pools and their impact on cellular metabolism and DNA
326 integrity. Kinetic analysis of the recombinant proteins showed that both 5'-HDNT and HAD2 are
327 5'-nucleotidases with primary activity on pyrimidine dNMPs, and thus are positioned to contribute
328 to recycling of pyrimidine pools in the cell. HAD2 strongly preferred dTMP, and 5'-HDNT, while
329 showing broad activity on dNMPs, was distinguished by having high activity on dCMP, suggesting
330 a non-redundant role. HAD1 was less active on these substrates and may instead be involved in
331 metabolism of trinucleotide substrates. Of the characterized enzymes, only 5'-HDNT was essential
332 for *T. brucei* blood stage growth. Knockdown of 5'-HDNT was associated with depletion of *de*
333 *novo* pyrimidine pathway intermediates, including L-Gln, sugar nucleotides, and phospholipids,
334 with a block in L-Gln uptake, any of which could be sufficient to lead to cell death. However, we
335 also observed altered nucleotide ratios and associated DNA damage. Taken together, these
336 findings support the essential role of the TK/5'-nucleotidase cycle in facilitating nucleoside and
337 nucleotide interconversion, allowing the U, T, and C pools to be exchanged to maintain the needed
338 ratios of pyrimidine and purine nucleotides. Disruption of this cycling pathway leads to aberrant

339 dNTP ratios, DNA damage, downregulation of L-Gln uptake, and cell death. We propose a model
340 whereby DNA damage in the context of disruptions in pyrimidine homeostasis signals the cell to
341 downregulate L-Gln transport by reducing transporter levels via a yet unidentified signaling
342 pathway (Fig 10).
343
344 HD and HAD protein superfamilies are metal-dependent enzymes that catalyze a wide range of
345 chemistries, including hydrolase reactions on multiple substrates [28-30]. In *T. brucei* we have
346 shown that members from both families encode 5'-nucleotidase activity. 5'-HDNT is a homolog
347 of the *E. coli* enzyme YfbR from the HD family, which also has a substrate preference towards
348 pyrimidine dNMPs [13]. *T. brucei* 5'-HDNT exhibits a similar substrate profile showing highest
349 activity towards pyrimidine dNMPs (dCMP, dUMP, and dTMP). HAD2 catalyzed similarly
350 efficient nucleotidase activity but with more limited substrate range, greatly preferring dTMP, with
351 a secondary activity on dAMP. 5'-HDNT was unique among the studied enzymes in showing high
352 activity towards dCMP. In contrast, HAD1 prefers C and G triphosphate substrates, and thus is
353 likely to play an alternative role in the pathway or in the cell. In fact, HAD domain proteins have
354 been reported to perform diverse biological functions beyond metabolic pool regulation, including
355 cellular maintenance, enzyme regulation, and nutrient uptake [28, 29]. The human genome
356 contains at least six characterized intracellular nucleotidases with varying substrate specificities,
357 cellular localizations, and cellular functions, and all are from the HAD superfamily [31]. Human
358 mitochondrial nucleotidases have been reported to form metabolic cycles with mitochondrial TK
359 but their physiological roles appear redundant given the availability of multiple routes to regulate
360 nucleotide pools in mammalian cells, including via the DCTD pathway [31-34]. A human HD
361 domain-containing protein (SAMHD1) has been reported to regulate dNTP levels, but it is a

362 triphosphatase rather than a nucleotidase [35, 36]. Knockout of a *T. brucei* paralog of SAMHD1
363 led to thymidine auxotrophy and to an increase in dCTP, suggesting a similar role to the
364 mammalian enzyme [37].
365
366 5'-HDNT and HAD2 catalyze dephosphorylation of TK products (dTMP and dUMP) along with
367 dCMP and thus are positioned to promote the cycling pathway that allows exchange between the
368 T and C nucleotide pools in *T. brucei*. The *T. brucei* TK knockout was rescued by expression of
369 *Hs*DCTD, which provides a route for direct conversion of dUMP to dCMP, a pathway that is
370 lacking in *T. brucei* [10]. Our finding that 5'-HDNT is essential and that the 5'-HDNT knockout
371 is also rescued by expression of *Hs*DCTD supports the conclusion that 5'-HDNT is involved in a
372 metabolic cycle with TK. To test this hypothesis further we generated a TK/5'-HDNT conditional
373 double knockout strain to determine if removing both enzymes could restore cell viability. We
374 found instead that simultaneous knockout of both proteins was lethal, with metabolite analysis
375 showing depletion of dTTP, similar to the effect of TK knockout alone [10]. These results suggest
376 that other 5'-nucleotidases are also contributing to the metabolic cycle with TK, and HAD2 is a
377 likely candidate for this role given its strong preference for dTMP as a substrate. While 5'-HDNT,
378 HAD2 and to some extent HAD1 show overlapping substrate specificity, 5'-HDNT is unique in
379 showing high activity on dCMP, and its ability to dephosphorylate this substrate with a relatively
380 low K_M appears to represent a non-redundant activity that contributes to its essentiality. Rescue of
381 5'-HDNT null cells by *Hs*DCTD further supports this hypothesis, as it also provides a pathway to
382 exchange the C nucleotide pools into the T and U pools.
383

384 The metabolic consequences of 5'-HDNT knockout included decreased pyrimidine triphosphate
385 nucleotide levels (dTTP and dCTP), which led to perturbed ratios of these nucleotides with their
386 purine base pair partners. Changes in nucleotide ratios have been shown to cause DNA damage in
387 mammalian and yeast cells [16, 17, 19, 20], and we reported this finding in *T. brucei* using two
388 orthologous methods to assess DNA damage. Compared to other mutagenic mechanisms affecting
389 DNA replication, nucleotide imbalance has been reported to cause mostly misinsertion and
390 misalignment errors, creating single-strand DNA breaks (SSBs) that progress to double strand
391 breaks (DSBs) with prolonged nucleotide stress [19, 38]. The alkaline comet assay can identify a
392 variety of DNA lesions, including SSBs, DSBs, and alkali-labile sites but cannot differentiate
393 between them [39, 40]. Similarly, the PCR-based assay we used to identify DNA lesions reveals
394 damage as a result of any process that induces polymerase stalling [22], which includes the damage
395 factors above. While the exact mechanism of DNA damage is unknown, our assays captured a
396 range of general processes that can promote genomic instability in the absence of 5'-HDNT.
397
398 Targeted metabolomics analysis found that in addition to the altered ratios between pyrimidine
399 and purine nucleotides, 5'-HDNT knockdown was associated with a substantial decrease in
400 intracellular L-Gln levels. This result was surprising given the abundance of L-Gln in *T. brucei*
401 growth media, suggesting a parasite-specific response to cope with the nucleotide metabolic
402 imbalance and DNA damage. In mammalian cells, there is increased flux through amino acid
403 uptake pathways to access more nutrients during times of stress or DNA damage, mainly through
404 mTORC1 activation [41, 42]. In contrast, we found that *T. brucei* responded by shutting down L-
405 Gln uptake, which then led to downstream depletion of *de novo* pyrimidine metabolic
406 intermediates and reduced pools of nucleotide sugars and lipids. This effect does not appear to be

407 a generalized response to cell growth arrest based on the finding that reduced L-Gln levels were
408 not observed in our TK c-null cell lines [10], in the reported null lines of the SAMHD1 homolog
409 despite its role in dephosphorylating nucleotides [37], nor in the double TK/5'-HDNT c-null cells
410 described herein. Additionally, published metabolomic profiling collected after treatment with
411 eflornithine, nifurtimox, or suramin suggests that treatment with these drugs did not impact L-Gln
412 levels [43, 44]. *De novo* glutamine synthesis has been reported in other trypanosomatids through
413 the glutamine synthetase enzyme [45, 46]. *T. brucei* encodes a putative glutamine synthetase, but
414 it has not been characterized, and our findings suggest that this pathway is unable to compensate
415 for the loss of glutamine uptake. While the signaling pathway that leads to downregulation of L-
416 Gln transport is unclear, it likely differs significantly from the response in mammalian cells. It is
417 notable that while some components of TOR complexes have been described in *T. brucei* [47-49],
418 many others are lacking, including the key mTOR activator protein kinase B (PKB/Akt) pathway
419 and well-studied mTOR effectors S6K and 4EBP1 [50, 51]. Furthermore, the current
420 understanding of cell death pathways in *T. brucei* is limited by the lack of identification of key
421 genes [52, 53]. For example, *T. brucei* is reported to contain apoptotic-like processes, but they lack
422 many canonical apoptotic players, including caspases and Bcl-2 family regulators [53, 54]. These
423 differences between trypanosomatids and other eukaryotes reveal divergence in mediating
424 metabolic and cellular responses, and the physiological relevance of programmed cell death in
425 trypanosomatids remains unclear. Our findings are consistent with a model where compromised *T.*
426 *brucei* cells initiate cell death by blocking L-Gln transport, thereby preserving nutrients for other
427 cells, especially given reports that L-Gln is consumed in large quantities from growth media [55,
428 56].
429

430 Through our study of 5'-HDNT, we have unmasked a potential cell death pathway in *T. brucei*
431 that we postulate maybe be activated in response to DNA damage. TK and 5'-HDNT function
432 together to form a critical metabolic cycle that allows interconversion between nucleotide
433 monophosphates and nucleosides. This cycle allows *T. brucei* to maintain a balance between the
434 C and T pyrimidine nucleotide pools and in turn with their purine counterparts. This pathway is
435 particularly important given the lack of other metabolic enzymes that are present in other
436 eukaryotic cells that can fulfill this function. The cellular requirement for dNTP/deoxynucleoside
437 interconversion likely serves multiple purposes, including providing an outlet for excess
438 metabolites to be recycled, maintaining tight regulation of nucleotide resources, and rendering
439 those metabolites available for other cellular functions. We propose that the loss of 5'-HDNT
440 causes a reduction in pyrimidine interconversion in *T. brucei*, leading to dNTP imbalance and
441 DNA damage, which in turn signals the cell to shut down L-Gln transport via an unknown
442 mechanism (Fig 10). Through this work, we have discovered a unique cellular response to the
443 disruption of pyrimidine balance related to nutrient availability, amino acid uptake, and DNA
444 integrity, thereby implicating multiple pathways for potential therapy development.

445 **Materials and Methods**

446

447 **Gene accession numbers**

448 *T. brucei* gene sequences were obtained from TriTrypDB [57, 58] using the following accession
449 numbers: HD domain 5'-nucleotidase (5'-HDNT): Tb927.9.10830, HAD domain phosphatase
450 (HAD1): Tb927.8.7510, HAD domain hydrolase (HAD2): Tb927.9.10500, thymidine kinase (TK):
451 Tb927.10.880, and TERT: Tb927.11.10190. The accession number for *Hs*DCTD is P32321 from
452 UniProt.

453

454 **Cloning, expression, and purification of recombinant *T. brucei* 5'-nucleotidases in *E. coli*.**
455 *Cloning of expression constructs*. Full-length nucleotidase genes were codon optimized,
456 synthesized by GenScript, and provided in a pUC57 vector. The 5'-HDNT and HAD1 genes were
457 extracted by generating a PCR product containing 5'BamHI and 3'XhoI restriction sites, which
458 were used to clone the resulting products into the pET-28b vector modified to contain a TEV
459 protease cleavage site following the N-terminal 6xHis tag (pET-28b-TEV) [59]. For HAD2, the
460 generated PCR product removed the N-terminal sequence (HAD2_Δ1-136) to generate a plasmid
461 that encoded the truncated enzyme. Cloning primers were as follows: 5'-HDNT primers p1/p2;
462 HAD1 primers p3/p4; HAD2 primers p5/p6 (S8 Table). Resultant clones were sequenced in their
463 entirety across the coding region and transfected into BL21(DE3) cells (Invitrogen).

464

465 *Protein expression and purification*. BL21(DE3) cells were cultured in 4 L Terrific Broth (RPI)
466 media with kanamycin (50 µg/mL) at 37°C until OD_{600} reached 0.8, then induced with 500 µM
467 isopropyl β-D-1-thiogalactopyranoside (IPTG) at 16°C for 16 h. Cells were harvested by

468 centrifugation then resuspended in buffer A (100 mM HEPES pH 8, 150 mM NaCl, 5 mM
469 imidazole, 5% glycerol, 5 mM 2-mercaptoethanol) with protease inhibitor cocktail (Roche) and 2
470 mM phenylmethylsulfonyl fluoride (PMSF). Cells were lysed using a cell disruptor and then
471 centrifuged at 20,000xg for 1 h at 4°C to remove cell debris. The soluble fraction was applied to a
472 HisTrap HP column (5 mL) (GE Healthcare) and eluted using a 5-45% gradient of buffer B (100
473 mM HEPES pH 8, 150 mM NaCl, 500 mM imidazole, 5% glycerol, 5 mM 2-mercaptoethanol).
474 Fractions containing the His-tagged nucleotidases were pooled and concentrated using an Amicon
475 10 kDa MWCO filter (Millipore). The protein was buffer-exchanged into gel filtration buffer (100
476 mM HEPES pH 7.4, 150 mM NaCl, 5% glycerol, 2 mM TCEP) and applied to a HiLoad 16/600
477 Superdex 200 pg column (GE Healthcare), and protein purity was assessed by SDS-PAGE. Protein
478 concentration was determined using the BCA Protein Assay Kit (Pierce) using bovine serum
479 albumin (BSA) to generate a standard curve.
480

481 **Steady-state kinetic analysis of 5'-nucleotidase activity**

482 Activity of purified 5'-nucleotidases was determined using a colorimetric endpoint assay for
483 phosphate quantitation as previously described [10]. Each reaction (50 µL) contained enzyme (20
484 nM or 40 nM), substrate (0-10 mM), and metal (0.5 mM $CoCl_2$ or 5 mM $MgCl_2$) in assay buffer
485 (50 mM HEPES pH 7.5) incubated at 37°C for 5, 10, or 20 min. For kinetic studies, reactions were
486 either mixed with 100 µL of BIOMOL Green detection reagent (Enzo Life Sciences) or for the
487 most active substrates, first diluted 1:10 in assay buffer before mixing with the BIOMOL reagent.
488 After 20 min at room temperature, absorbance at 620 nm was measured. Absorbance values were
489 converted to µM phosphate using a phosphate standard curve ranging from 0-25 µM (Cayman
490 Chemical). Rate data were obtained by taking the slope across the linear portion of the time curve

491 (0, 5, 10, and 20 min timepoints). Preliminary studies were conducted to confirm linearity over
492 various concentrations of enzyme (0-100 nM) and substrate (0-2 mM) monitored from 0-15 min.
493 Enzyme kinetic data were analyzed using GraphPad Prism v9.4.0 using the Michaelis-Menten
494 model and fit using the following equation: $V_0 = V_m[S]/(K_M + [S])$, where V_0 is the initial velocity,
495 V_m is the maximum velocity, [S] is the substrate concentration, and K_M is the Michaelis constant
496 for each substrate. The k_{cat} was calculated from the V_m and the enzyme concentration. The molar
497 absorptivity of malachite green at 620 nm is 1.49 x 10^5 M^{-1} cm^{-1}.
498
499 ***T. brucei* culture**
500 Wild-type cells used in this study were *T. brucei* bloodstream form single marker (SM) cells that
501 constitutively express the *Tet* repressor and T7 RNA polymerase, both maintained with Geneticin
502 (G418) (2.5 µg/mL) [60]. *T. brucei* cells were grown in HMI-19 medium supplemented with 10%
503 fetal bovine serum (FBS) or dialyzed FBS (dFBS) at 37°C and 5% CO_2 as described [10, 61].
504 HMI-19 is a modified media with physiological levels of nucleotide precursors and contains no
505 added hypoxanthine nor thymidine except what is present in the serum. In the case of media made
506 using dFBS, media was supplemented with 10 µM hypoxanthine to provide the cell with needed
507 purines. Cell density was maintained between 10^5-10^6 cells/mL for exponential growth. 5'-HDNT,
508 HAD1, and HAD2 knockout lines were cultured in the appropriate antibiotics at the following
509 concentrations: 2.5 µg/mL G418 (Life Technologies), 2.5 µg/mL hygromycin (Sigma), 0.1 µg/mL
510 puromycin (Sigma), 2.5 µg/mL phleomycin (InvivoGen), 2.5 µg/mL blasticidin (InvivoGen), and
511 1 µg/mL tetracycline (Tet) (RPI). Conditional knockout lines were supplemented with 1 µg/mL
512 Tet daily to maintain expression of Tet-regulated proteins. Prior to initiating growth curves and
513 analysis in the absence of Tet, parasites were centrifuged at 2500xg for 5 min at room temperature

514 and washed three times with warm (37°C) media (FBS or dFBS) (0.5 mL/10^6 cells) before seeding
515 in media without Tet or selection antibiotics. For growth analyses, cells were then seeded at 50,000
516 cells/mL. Cell counts were collected daily using a hemocytometer (Bright-Line), and then cells
517 were diluted with fresh culture media to 10^5 cells/mL. The limit of detection is 10^4 cells.
518

519 **Western blot and capillary immunoassay**

520 Expression of FLAG-tagged 5'-HDNT, *Hs*DCTD, and TK was analyzed by traditional Western
521 blot or capillary-based Western assays. Parasites (10^6-10^7) were harvested by centrifugation at
522 2500xg for 5 min, washed once with cold phosphate buffered saline (PBS) (137 mM NaCl, 2.7
523 mM KCl, 8 mM Na_2HPO_4, and 2 mM KH_2PO_4 pH 7.4), and resuspended in 50 µL lysis buffer (50
524 mM HEPES pH 8, 150 mM NaCl, 3 mM TCEP, 2 mM PMSF, 1 mg/mL leupeptin, 2 mg/mL
525 antipain, 10 mg/mL benzamidine, 1 mg/mL pepstatin, 1 mg/mL chymostatin). Cells were lysed by
526 three freeze-thaw cycles, and cell debris was removed by centrifugation at 16,000xg for 10 min at
527 4°C. The soluble fraction was collected, and protein concentration was determined using the BCA
528 Protein Assay Kit (Pierce) using BSA to generate a standard curve. For traditional Western blot
529 studies, 30 µg of protein was resolved on a 12.5% SDS-PAGE gel and transferred to a
530 nitrocellulose membrane. Membranes were incubated for 1 h at 4°C in blocking buffer containing
531 5% nonfat dry milk in Tris-buffered saline (20 mM Tris pH 7.6, 150 mM NaCl) and 0.1% Tween-
532 20 (TBS-T). The membrane was then incubated in primary antibody in 5% milk and TBS-T
533 overnight at 4°C at the following dilutions: 1:1000 rabbit αFLAG polyclonal (Invitrogen) and
534 1:1000 rabbit αHsp70 polyclonal (Abcam). Membranes were washed three times (5 min each)
535 with TBS-T, incubated with the secondary antibody Protein A-HRP (Abcam) at 1:10000 dilution
536 for 1 h at room temperature, washed three times (5 min each) with TBS-T, and then incubated in

537 SuperSignal West Pico Chemiluminescent Substrate (Thermo Fisher) for 5 min and visualized
538 using an ImageQuant LAS 400 imager (Cytiva).
539
540 For the capillary-based Western assay using the Jess platform (ProteinSimple), cell lysate was
541 diluted to 0.1 mg/mL, prepared according to the manufacturer's instructions, and separated using
542 a 12 – 230 kDa separation module (ProteinSimple). The following primary antibody dilutions were
543 used: 1:250 rabbit αFLAG polyclonal (Invitrogen) and 1:50 rabbit αHsp70 polyclonal (Abcam).
544 The secondary antibody was anti-rabbit HRP (ProteinSimple). For total protein normalization, the
545 total protein detection module (ProteinSimple) was prepared according to the manufacturer's
546 instructions in place of the αHsp70 probe. All data were analyzed using Compass Software v5.0.1
547 (ProteinSimple).
548
549 **mRNA quantitation by qPCR**
550 RNA purification, cDNA synthesis, and qPCR analysis was carried out as previously described
551 [62]. Briefly, total RNA was extracted from 10^7 parasites using TRIzol reagent (Invitrogen) and
552 the RNeasy Mini Kit (Qiagen) according to the manufacturer's protocol. The RNA was treated
553 with DNase I (Invitrogen) and transcribed to cDNA using SuperScript IV Reverse Transcriptase
554 (Invitrogen). Relative mRNA quantitation was performed using the iTaq Universal SYBR Green
555 Supermix (Bio-Rad) using a standard curve of wild-type mRNA for each primer set and *TERT* as
556 a reference gene. Primers used are as follows: 5'-HDNT primers p7/p8; HAD1 primers p9/p10;
557 HAD2 primers p11/p12; *TERT* primers p13/p14 (S8 Table). Data was collected on a CFX384
558 Touch Real-Time PCR machine (Bio-Rad), and quantification cycle (C_q) values were determined
559 using the CFX Maestro software v2.1 (Bio-Rad). Data was analyzed using the Pfaffl method [63].

560

561 **Generation of *T. brucei* null and c-null cell lines for 5'-HDNT, HAD1, and HAD2**

562 Genomic DNA was isolated from SM cells ($5x10^7$) using the DNeasy Blood and Tissue Kit
563 (Qiagen) according to the manufacturer's instructions. Flanking 5' and 3' regions for each
564 nucleotidase or TK gene were amplified from SM wild-type genomic DNA and fused to
565 hygromycin or puromycin resistance genes by fusion PCR as described [64] using primers p15-
566 p38 as provided in S8 Table. The hygromycin resistance gene was amplified from the pLew90
567 vector [60] (primers p39/p40) and puromycin resistance gene from a codon-optimized puromycin
568 gene in a vector synthesized by GenScript as previously described (primers p41/p42) [10]. Fusion
569 PCR products were gel-purified by the QIAquick PCR & Gel Cleanup Kit (Qiagen). For Tet-
570 regulated rescue constructs, N-terminal FLAG-tagged 5'-HDNT or *Hs*DCTD genes were
571 subcloned into pLew100v5 [60] using BamHI and HindIII and the following primers: 5'-HDNT
572 primers p43/p44; *Hs*DCTD primers p45/p46 (S8 Table). The 5'-HDNT conditional knockout cell
573 lines (c-null) were generated by first replacing one allele with hygromycin followed by the
574 introduction of a Tet-regulated 5'-HDNT or *Hs*DCTD expression construct. The second 5'-HDNT
575 allele was then replaced with puromycin, creating the 5'-HDNT c-null lines, 5'-HDNT$^{-/-}$Tet(5'-
576 HDNT) or 5'-HDNT$^{-/-}$Tet(*Hs*DCTD). Parasite transfections were performed as previously
577 described [10]. PCR product (1 µg) or NotI-linearized rescue plasmid (5 µg) was ethanol
578 precipitated and resuspended in 10 µL water. Parasites ($2x10^7$) in Human T Cell Nucleofector
579 Solution (100 µL) (Lonza) were transfected using the Amaxa Nucleofector machine (Lonza) using
580 protocol X-001 and transferred to media (50 mL) to recover for 6 h. Parasites were diluted (1:25
581 and 1:50) into media with selection appropriate selection antibiotics in 48-well plates at 1 mL/well.

582 Negative control parasites transfected with empty vector were included and monitored throughout.
583 After 4 days, wells with 10^6 cells/mL were cloned by limiting dilution.
584

585 **Generation of *T. brucei* TK/5'-HDNT double c-null cell line**

586 Given the limited number of resistance markers available and the essentiality of both TK and 5'-
587 HDNT, the double TK/5'-HDNT knockout c-null line was achieved using a Cre recombinase
588 system [65] with Tet-regulated rescue constructs for TK and 5'-HDNT generated as described
589 above. The first allele of 5'-HDNT was replaced by antibiotic resistance marker hygromycin fused
590 to herpes simplex virus thymidine kinase (HSV-TK) and flanked by loxP sites (hyg-HSV-TK-
591 loxP). The hyg-HSV-TK-loxP cassette was amplified from the pHJ17 plasmid (Addgene) [65]
592 using primers p47/p48 (S8 Table). The 5' and 3' flanking regions were amplified from wild-type
593 SM cells using primers p15/p49 and p16/p50, respectively. The pLew100v5-based rescue
594 construct of Tet-regulated 5'-HDNT was transfected and selected using phleomycin. The second
595 5'-HDNT allele was replaced by a similar puromycin cassette (puro-HSV-TK-loxP) amplified
596 from the pHJ18 plasmid (Addgene) [65] using primers p47/p48. To recover the two antibiotic
597 markers, cells were transfected with pLew100cre-del-tetO (Addgene) [66] and selected with 40
598 µg/mL ganciclovir. The recycled hygromycin and puromycin markers were then used to generate
599 the conditional knockout of *T. brucei* TK (primers p51-p58) as described above using a
600 pLew100v5-based rescue construct with blasticidin selection instead of phleomycin [67].
601

602 **Metabolomic analysis of *T. brucei* cell lines**

603 5'-HDNT c-null cells expressing either 5'-HDNT, *Hs*DCTD or both 5'-HDNT and TK (double
604 KO line) were grown as described above with or without Tet for 48 h. HAD1 and HAD 2 null lines

605 were grown in the absence of Tet and compared to the wild-type SM strain. Parasites (10^8) were
606 immersed in a dry ice/ethanol bath until the temperature reached 4°C. Cells were harvested by
607 centrifugation (2500xg, 5 min, 4°C), washed three times with cold PBS (25 mL), and resuspended
608 in 250 µL cold (-80°C) 80% methanol. Cells were vortexed and lysed by freeze-thawing three
609 times in liquid nitrogen. Cell debris was pelleted by centrifugation at 16,000xg for 20 min at 4°C.
610 The supernatant was isolated and analyzed by LC-MS/MS. Total protein in the cell pellet was
611 quantitated using the BCA Protein Assay Kit (Pierce) and used for data normalization.
612
613 To detect a broad range of metabolites, samples were analyzed using multiple ion modes and
614 chromatography methods. Mass spectrometric analyses were performed on a Sciex QTRAP 6500+
615 mass spectrometer equipped with an electrospray ion (ESI) source. The ESI source was used in
616 both positive and negative ion modes, configured as follows: Ion Source Gas 1 (Gas 1), 40 psi; Ion
617 Source Gas 2 (Gas 2), 35 psi; curtain gas (CUR), 50 psi in the negative polarity mode and 45 psi
618 in the positive polarity mode; source temperature, 550°C; and ion spray voltage (IS), +4800 V(+)
619 and −4500 V(−). The mass spectrometer was coupled to a Shimadzu HPLC (Nexera X2 LC-30AD).
620 The system was controlled by Analyst 1.7.2 software. Hydrophilic interaction liquid
621 chromatography was performed using a SeQuant ZIC-pHILIC 5 µm polymeric 150 × 2.1 mm
622 PEEK coated HPLC column (Millipore Sigma). The column temperature, sample injection volume,
623 and flow rate were 45°C, 5 µL, and 0.15 mL/min respectively. HPLC conditions were as follows:
624 Solvent A: 20 mM ammonium carbonate with 0.1% ammonium hydroxide; Solvent B: acetonitrile.
625 The gradient pattern was 0 min: 80% B, 20 min: 20% B, 20.5 min 80% B, 34 min: 80% B.
626

627 Reverse phase chromatography was performed using an ACE 3 C18-PFP 150 x 4.6 mm HPLC
628 column (Mac-Mod). The ESI source was configured as above except the ion spray voltage as
629 follows: +5500 V(+) and −4500 V(−). Column temperature, sample injection volume, and flow
630 rate were 30°C, 5 µL, and 0.5 mL/min respectively. HPLC conditions were as follows: Solvent A:
631 water with 0.1% formic acid (v/v), LC-MS grade and Solvent B: acetonitrile with 0.1% formic
632 acid (v/v), LC-MS grade. Gradient conditions were 0-2 min: 5% B, 5-16 min: 90% B, 17 min 5%
633 B, 30 min: 5% B. All data were processed using MultiQuant 3.0.3 software with relative
634 quantification based on the peak area of each small molecule.
635
636 The calculated peak areas were normalized to amount of total protein in each sample pellet. To
637 determine the relative abundance of each metabolite, the peak area in the -Tet condition was
638 normalized to the +Tet signal, and volcano plots were generated using GraphPad Prism v9.4.0 with
639 *p* values calculated from 3-4 technical replicates per condition. Statistical significance was
640 determined in GraphPad Prism using multiple T-test analysis without correction for multiple
641 comparisons. Independent biological replicates were collected as described in figure legends.
642
643 **Quantitation of dNTP levels by a PCR-based fluorescence assay**
644 Quantitation of intracellular dNTPs was achieved using a fluorescence-based assay described in
645 [68]. The assay uses Taq polymerase-based extension on an oligonucleotide template annealed
646 with a dual-quenched (ZEN and IBFQ) 6-FAM fluorophore-labeled probe that generates a
647 fluorescence signal proportional to dNTP concentration. Cells were grown with or without Tet for
648 48 h to a density of 10^6 cells/mL, and 10^7 total cells were centrifuged at 2500xg for 5 min. Cells
649 were washed once in cold PBS, resuspended in 250 µL 60% methanol, then stored at -20°C

650 overnight. Samples were boiled in a 100°C heat block for 5 min and centrifuged at 16,000xg for
651 20 min at 4°C. Total protein in the pellet was quantitated using the BCA Protein Assay Kit (Pierce).
652 The supernatant containing extracted dNTPs was separated into a new 1.7 mL tube and dried by
653 speed vacuum. The resulting pellet was resuspended in 50 µL assay buffer (1x Taq PCR buffer
654 and 2 mM $MgCl_2$). Each reaction was 25 µL and contained 400 nM NDP1 primer, 400 nM
655 oligonucleotide template, 400 nM fluorophore-labeled probe, 100 µM dNTP mix (Invitrogen),
656 1.25 units PlatinumTaq DNA polymerase (Invitrogen), and 2.5 µL or 5 µL of dNTP extract to
657 confirm linearity. Fluorescence measurements were collected on a CFX384 Touch Real-Time PCR
658 machine (Bio-Rad) using the following program: initial denaturation at 94°C for 2 min, then 8
659 cycles of extension at 60°C for 5 min with fluorescence reading. Standard curves were generated
660 with 0-5 pmol dNTP (Sigma). All detection probes, oligonucleotide templates, and the NDP1
661 primer used in this assay are listed in [68] and were purchased from Integrated DNA Technologies.
662

663 **L-Gln uptake assays**

664 Parasites (10^7-10^8) were centrifuged at 2500xg for 5 min and washed twice in warm Carter's
665 balanced saline solution (CBSS), as described in [43], before resuspending in CBSS. Uptake
666 assays were performed using a described spin through oil method to allow separation of free label
667 from cells over short time intervals [15]. Silicone oil AR 20/200 mix (density = 1.035 g/mL)
668 (Sigma) (100 µL) was pipetted into 1.7 mL tubes and was then layered with 150 µL of $^{13}C_5$ $^{15}N_2$-
669 L-Gln (Cambridge Isotope Laboratories) to yield a final concentration of 50 µM when mixed with
670 cells. $^{13}C_5$-L-ornithine (Cambridge Isotope Laboratories) was used as a control at a final
671 concentration of 100 µM. Cells ($5x10^6$ total cells) (1 mL) were added to each tube in 20 s
672 increments followed by immediate centrifugation at max speed for 30 s to separate the cells from

673 the labeled L-Gln. The aqueous portion above the oil was removed by aspiration followed by two
674 1-mL PBS washes of the oil layer. Oil was removed, and cells were resuspended in 500 µL 80%
675 methanol for metabolite extraction. Cells were lysed by three cycles of freeze-thaw in liquid
676 nitrogen and centrifuged at 16,000xg at 4°C for 15 min. The supernatant was dried by speed
677 vacuum and resuspended in 50% acetonitrile/30% methanol/20% water (v/v). For quantitation of
678 labeled L-Gln, a 12-point standard curve was generated in a matrix of dilute cell lysate, dried by
679 speed vacuum, and resuspended as above.
680
681 Metabolites were analyzed by LC-MS/MS using an AB Sciex 6500+ QTRAP mass spectrometer
682 coupled to a Shimadzu Nexera X2 LC. LC method details are as described in [69] with the injection
683 volume varying from 5-15 µL. Compounds were detected with the mass spectrometer in the
684 negative multiple reaction monitoring mode by following the precursor to fragment ion transitions
685 below: glutamine: *m/z* 145 → *m/z* 127; *m/z* 145 → *m/z* 109; glutamate: *m/z* 146 → *m/z* 128; *m/z*
686 146 → *m/z* 102.1; $^{13}C_5{}^{15}N_2$ glutamine / $^{13}C_5{}^{15}N_1$ glutamate: *m/z* 152 → *m/z* 134; $^{13}C_5{}^{15}N_2$ glutamine
687 *m/z* 152 → *m/z* 116; $^{13}C_5{}^{15}N_1$ glutamate *m/z* 152 → *m/z* 107.1; succinate: *m/z* 117 → *m/z* 99; *m/z*
688 117 → *m/z* 73; $^{13}C_4$ succinate: *m/z* 121 → *m/z* 103; *m/z* 121 → *m/z* 76. Ornithine was analyzed by
689 the same LC-MS/MS system in the positive multiple reaction monitoring mode by following the
690 precursor to fragment ion transitions below: ornithine: *m/z* 133 → *m/z* 70; *m/z* 133 → *m/z* 116;
691 $^{13}C_5$ ornithine: *m/z* 138.1 → *m/z* 74.2; m/z 138.1 → 121. Retention times were as follows:
692 glutamine and $^{13}C_5{}^{15}N_2$ glutamine: 4.59 min; glutamate and $^{13}C_5{}^{15}N_1$ glutamate: 4.68 min;
693 succinate and $^{13}C_4$ succinate: 3.76 min; ornithine and $^{13}C_5$ ornithine: 3.85 min. An Acquity UPLC
694 BEH Amide (2.1x100 mm, 1.7 µm particles) column was used to chromatographically separate
695 ornithine with the following conditions, adapted from [70]: mobile phase A – water with 0.1%

696 formic acid; mobile phase B – acetonitrile with 0.1% formic acid; 0-0.1 min. 85% B, 0.1-5min.
697 85-55% B, 5-7 min. 55-30% B, 7-8 min. 30% B, 8-8.5 min. 30-0% B, 8.5-9 min. 0% B, 9-10 min.
698 0-85% B, 10-13 min. 85% B; flow rate 0.35 ml/min.; 5 µL injection volume; 4°C autosampler
699 temperature; 50°C column temperature. A Thermo Scientific BioBasic AX (2.1 x 50 mm, 5 µm
700 particles) column was used to chromatographically separate UMP with the following conditions:
701 mobile phase A - water/acetonitrile (70/30; v/v) with 10 mM ammonium acetate pH 6; mobile
702 phase B - water/acetonitrile (70/30; v/v) with 1 mM ammonium acetate pH 10.5; 0-1 min. 0% B,
703 1-2.5 min. 0-35% B, 2.5-5 min. 35% B, 5-7 min. 35-65% B, 7-8.5 min. 65% B, 8.5-9 min. 65-100%
704 B, 9-13.5 min. 100% B, 13.5-14 min. 100-0% B, 14-19 min. 0% B; flow rate 0.5 mL/min.; 5 µL
705 injection volume; 4°C autosampler temperature; 30°C column temperature. UMP isotopes were
706 detected with the mass spectrometer in the positive multiple reaction monitoring mode by
707 following the precursor to fragment ion transitions below: UMP: *m*/*z* 325.1 → *m*/*z* 97; UMP M+1:
708 *m*/*z* 326.1 → *m*/*z* 97 (the M+1 isotope represents the labeled $^{15}N_1$-UMP as well as naturally
709 occurring isotopes). Retention times were as follows: UMP: 5.36 min; UMP M+1: 5.78 min. All
710 paired transitions between isotopes had identical declustering potentials, entrance potentials,
711 collision energies, and collision cell exit potentials. Retention times were verified by injections of
712 individual compound standards. All LC-MS/MS data was quantitated in AB Sciex MultiQuant
713 v.3.0.3 software. Data is reported either as pmoles/10^6 cells (for glutamine only) or as percent
714 labeled, calculated as the ratio of peak areas between the labeled compound and the sum of labeled
715 with unlabeled compound as described without correction for natural isotope abundance [71].
716
717 **Detection of DNA lesions by PCR**

718 DNA damage was assessed using a PCR-based technique described in [22] comparing relative
719 amplification levels between wild-type and knockout parasites. All cells in this assay were cultured
720 in FBS media containing 2.5 μg/mL G418 and no selection antibiotics. Knockout cells were grown
721 with or without Tet for 24, 36, or 48 h to a density of 10^6 cells/mL. All other cells were cultured
722 for 48 h. Positive control cells were treated with hydroxyurea (HU) (100 μM) (Sigma) or methyl
723 methanesulfonate (MMS) (0.002%) (Sigma) for 24 h prior to harvesting. Final cell density was
724 determined using a hemocytometer, and $5x10^7$ total cells were collected per condition. All cells
725 were centrifuged at 2500xg for 5 min, washed once with PBS, then processed using the DNeasy
726 Blood and Tissue kit (Qiagen) to extract gDNA. A 10 kb portion of the *T. brucei* genome was
727 amplified along with a smaller 200 bp fragment as a control for DNA loading using primers
728 previously described in [23] and provided in S8 Table: large fragment primers p59/p61; small
729 fragment primers p60/p61. The amplified region on chromosome 8
730 (Tb927_08_v5.1:988504..999214) spans multiple *T. brucei* genes (Tb927.8.3290, Tb927.8.3300,
731 Tb927.8.3310, Tb927.8.3320, and Tb927.8.3330) to capture expected lesions that are randomly
732 distributed along the genome. DNA amount was quantitated using the Quant-iT PicoGreen dsDNA
733 Assay Kit (Invitrogen), and 15 ng was used in each PCR reaction. PCR reactions were run until
734 product amplification was in the linear range. At this cycle number, fluorescence is directly
735 proportional to the amount of starting template. This parameter was determined to be 20 cycles in
736 our lab by measuring amplification with 15 ng and 7.5 ng of template DNA at various cycle
737 numbers. PCR products in control reactions were run on an agarose gel to ensure that only a single
738 band was generated. Amplified DNA was quantitated using the PicoGreen assay, and number of
739 DNA lesions was calculated as in [22]. Clinically used anti-trypanosomal drugs served as controls

740 using the following published EC_{50} values: 15 μM eflornithine (Sigma) [26], 2.5 nM pentamidine
741 (Sigma) [26], 27 nM suramin (Sigma) [26], and 1 μM fexinidazole (Sigma) [72, 73].
742

743 **Alkaline comet assay for detection of DNA damage**

744 All parasites were cultured in FBS media with selection antibiotics removed except 2.5 μg/mL
745 G418. Knockout cells were grown with or without Tet for 48 h. Positive control cells were treated
746 with MMS (0.002%) for 24 h prior to harvesting. Detection of DNA damage was then carried out
747 using a comet assay kit (Abcam). Briefly, parasites were spun at 2500xg for 5 min at room
748 temperature, washed once in PBS, and resuspended at 10^5 cells/mL. Cells were mixed with agarose
749 in a 1:5 (v/v) ratio, and 70 μL was carefully layered on top of 70 μL solidified agarose on a glass
750 slide. The slides were processed according to the manufacturer's instructions and imaged using a
751 fluorescent cell imager (Bio-Rad) and analyzed using an ImageJ plugin, OpenComet v1.3.1, to
752 automate comet selection and analysis [27]. The intensity of image pixels was used to determine
753 two parameters: tail length (length of the tail in pixels) and tail DNA percent (percentage of DNA
754 in tail). The tail moment was calculated as the product of tail length and tail DNA percent. For
755 each condition, 50 comets were analyzed. Images were manually inspected to confirm exclusion
756 of overlapping comets or other irregular regions.

757 **Acknowledgements.** The authors thank Dr. Anthony Davis for helpful discussion regarding DNA
758 damage and acknowledge resources and expertise provided by the Preclinical Pharmacology Core
759 at UT Southwestern. We also thank Drs. James Collins, Anthony Michael, and Dawn Wetzel for
760 critical reading of the manuscript. MAPh holds the Sam G. Winstead and F. Andrew Bell
761 Distinguished Chair in Biochemistry.

762

763 **Funding**

764 Research was supported by NIH NIAID grant R37AI034432 and R01AI034432 (to MAPh) and
765 T32GM127216 (to YWD and MAPo). MAPh acknowledges the support of the Welch Foundation
766 grant I-1257. The content is solely the responsibility of the authors and does not necessarily
767 represent the official views of the National Institutes of Health.

768

769 **Author Contributions**

770 **Yue Wen Deng:** Conceptualization, Investigation, Visualization, Writing – Original Draft,
771 Writing – Review & Editing.

772 **Michael A. Pontikos:** Investigation, Methodology, Writing – Review & Editing.

773 **Hamid Baniasadi:** Investigation, Writing – Review & Editing.

774 **Noelle S. Williams:** Supervision, Writing – Review & Editing.

775 **Margaret A. Phillips:** Conceptualization, Funding Acquisition, Supervision, Writing – Original
776 Draft, Writing – Review & Editing.

777

References

1. Morrison LJ, Steketee PC, Tettey MD, Matthews KR. Pathogenicity and virulence of African trypanosomes: From laboratory models to clinically relevant hosts. Virulence. 2023;14(1):2150445. doi: 10.1080/21505594.2022.2150445. PubMed PMID: 36419235; PubMed Central PMCID: PMC9815240.
2. WHO. Trypanosomiasis, human African (sleeping sickness) [Fact Sheet]. World Health Organization; 2022.
3. Kennedy PGE. Update on human African trypanosomiasis (sleeping sickness). J Neurol. 2019;266(9):2334-7. Epub 20190617. doi: 10.1007/s00415-019-09425-7. PubMed PMID: 31209574.
4. Kasozi KI, Zirintunda G, Ssempijja F, Buyinza B, Alzahrani KJ, Matama K, et al. Epidemiology of Trypanosomiasis in Wildlife-Implications for Humans at the Wildlife Interface in Africa. Front Vet Sci. 2021;8:621699. Epub 20210614. doi: 10.3389/fvets.2021.621699. PubMed PMID: 34222391; PubMed Central PMCID: PMC8248802.
5. Morrison LJ, Vezza L, Rowan T, Hope JC. Animal African Trypanosomiasis: Time to Increase Focus on Clinically Relevant Parasite and Host Species. Trends Parasitol. 2016;32(8):599-607. Epub 20160508. doi: 10.1016/j.pt.2016.04.012. PubMed PMID: 27167665.
6. De Koning HP. The Drugs of Sleeping Sickness: Their Mechanisms of Action and Resistance, and a Brief History. Trop Med Infect Dis. 2020;5(1). Epub 20200119. doi: 10.3390/tropicalmed5010014. PubMed PMID: 31963784; PubMed Central PMCID: PMC7157662.
7. Pai C-C, Kearsey SE. A Critical Balance: dNTPs and the Maintenance of Genome Stability. Genes. 2017;8(2). doi: 10.3390/genes8020057. PubMed Central PMCID: PMC5333046.
8. Ali JAM, Creek DJ, Burgess K, Allison HC, Field MC, Mäser P, et al. Pyrimidine salvage in Trypanosoma brucei bloodstream forms and the trypanocidal action of halogenated pyrimidines. Mol Pharmacol. 2013;83(2):439-53. doi: 10.1124/mol.112.082321. PubMed Central PMCID: PMC4857052.
9. Tiwari K, Dubey VK. Fresh insights into the pyrimidine metabolism in the trypanosomatids. Parasit Vectors. 2018;11(1):87. Epub 20180208. doi: 10.1186/s13071-018-2660-8. PubMed PMID: 29422065; PubMed Central PMCID: PMC5803862.
10. Leija C, Rijo-Ferreira F, Kinch LN, Grishin NV, Nischan N, Kohler JJ, et al. Pyrimidine Salvage Enzymes Are Essential for De Novo Biosynthesis of Deoxypyrimidine Nucleotides in Trypanosoma brucei. PLoS Pathog. 2016;12(11):e1006010. doi: 10.1371/journal.ppat.1006010. PubMed Central PMCID: PMC5098729.
11. Valente M, Timm J, Castillo-Acosta VM, Ruiz-Perez LM, Balzarini T, Nettleship JE, et al. Cell cycle regulation and novel structural features of thymidine kinase, an essential enzyme in Trypanosoma brucei. Mol Microbiol. 2016;102(3):365-85. Epub 20160831. doi: 10.1111/mmi.13467. PubMed PMID: 27426054.
12. Finn RD, Coggill P, Eberhardt RY, Eddy SR, Mistry J, Mitchell AL, et al. The Pfam protein families database: towards a more sustainable future. Nucleic Acids Res. 2016;44(D1):D279-85. Epub 20151215. doi: 10.1093/nar/gkv1344. PubMed PMID: 26673716; PubMed Central PMCID: PMC4702930.
13. Zimmerman MD, Proudfoot M, Yakunin A, Minor W. Structural insight into the mechanism of substrate specificity and catalytic activity of an HD-domain phosphohydrolase: the

822 5'-deoxyribonucleotidase YfbR from Escherichia coli. J Mol Biol. 2008;378(1):215-26. doi:
823 10.1016/j.jmb.2008.02.036. PubMed Central PMCID: PMC2504004.
824 14. Fenyk S, Campillo Ade S, Pohl E, Hussey PJ, Cann MJ. A nucleotide phosphatase activity
825 in the nucleotide binding domain of an orphan resistance protein from rice. J Biol Chem.
826 2012;287(6):4023-32. Epub 20111208. doi: 10.1074/jbc.M111.314450. PubMed PMID:
827 22157756; PubMed Central PMCID: PMC3281693.
828 15. Geddes EJ, Li Z, Hergenrother PJ. An LC-MS/MS assay and complementary web-based
829 tool to quantify and predict compound accumulation in E. coli. Nat Protoc. 2021;16(10):4833-54.
830 Epub 20210903. doi: 10.1038/s41596-021-00598-y. PubMed PMID: 34480129; PubMed Central
831 PMCID: PMC8715754.
832 16. Diehl FF, Miettinen TP, Elbashir R, Nabel CS, Darnell AM, Do BT, et al. Nucleotide
833 imbalance decouples cell growth from cell proliferation. Nat Cell Biol. 2022;24(8):1252-64. Epub
834 20220804. doi: 10.1038/s41556-022-00965-1. PubMed PMID: 35927450; PubMed Central
835 PMCID: PMC9359916.
836 17. Hastak K, Paul RK, Agarwal MK, Thakur VS, Amin AR, Agrawal S, et al. DNA synthesis
837 from unbalanced nucleotide pools causes limited DNA damage that triggers ATR-CHK1-
838 dependent p53 activation. Proc Natl Acad Sci U S A. 2008;105(17):6314-9. Epub 20080423. doi:
839 10.1073/pnas.0802080105. PubMed PMID: 18434539; PubMed Central PMCID: PMC2359797.
840 18. Kohalmi SE, Glattke M, McIntosh EM, Kunz BA. Mutational specificity of DNA precursor
841 pool imbalances in yeast arising from deoxycytidylate deaminase deficiency or treatment with
842 thymidylate. J Mol Biol. 1991;220(4):933-46. doi: 10.1016/0022-2836(91)90364-c. PubMed
843 PMID: 1880805.
844 19. Kumar D, Abdulovic AL, Viberg J, Nilsson AK, Kunkel TA, Chabes A. Mechanisms of
845 mutagenesis in vivo due to imbalanced dNTP pools. Nucleic Acids Res. 2011;39(4):1360-71. Epub
846 20101020. doi: 10.1093/nar/gkq829. PubMed PMID: 20961955; PubMed Central PMCID:
847 PMC3045583.
848 20. Kunz BA. Mutagenesis and deoxyribonucleotide pool imbalance. Mutat Res. 1988;200(1-
849 2):133-47. doi: 10.1016/0027-5107(88)90076-0. PubMed PMID: 3292903.
850 21. Kunz BA, Kohalmi SE, Kunkel TA, Mathews CK, McIntosh EM, Reidy JA. International
851 Commission for Protection Against Environmental Mutagens and Carcinogens.
852 Deoxyribonucleoside triphosphate levels: a critical factor in the maintenance of genetic stability.
853 Mutat Res. 1994;318(1):1-64. doi: 10.1016/0165-1110(94)90006-x. PubMed PMID: 7519315.
854 22. Santos JH, Meyer JN, Mandavilli BS, Van Houten B. Quantitative PCR-Based
855 Measurement of Nuclear and Mitochondrial DNA Damage and Repair in Mammalian Cells. In:
856 Henderson DS, editor. DNA Repair Protocols: Mammalian Systems. Totowa, NJ: Humana Press;
857 2006. p. 183-99.
858 23. Vieira-da-Rocha JP, Passos-Silva DG, Mendes IC, Rocha EA, Gomes DA, Machado CR,
859 et al. The DNA damage response is developmentally regulated in the African trypanosome. DNA
860 Repair (Amst). 2019;73:78-90. Epub 20181114. doi: 10.1016/j.dnarep.2018.11.005. PubMed
861 PMID: 30470509; PubMed Central PMCID: PMC6329875.
862 24. Phillips MA. Polyamines in protozoan pathogens. J Biol Chem. 2018;293(48):18746-56.
863 Epub 20181017. doi: 10.1074/jbc.TM118.003342. PubMed PMID: 30333232; PubMed Central
864 PMCID: PMC6290135.
865 25. Pegg AE. Introduction to the Thematic Minireview Series: Sixty plus years of polyamine
866 research. J Biol Chem. 2018;293(48):18681-92. Epub 20181030. doi: 10.1074/jbc.TM118.006291.
867 PubMed PMID: 30377254; PubMed Central PMCID: PMC6290159.

868 26. Thomas JA, Baker N, Hutchinson S, Dominicus C, Trenaman A, Glover L, et al. Insights
869 into antitrypanosomal drug mode-of-action from cytology-based profiling. PLoS Negl Trop Dis.
870 2018;12(11):e0006980. doi: 10.1371/journal.pntd.0006980. PubMed Central PMCID:
871 PMC6283605.
872 27. Gyori BM, Venkatachalam G, Thiagarajan PS, Hsu D, Clement MV. OpenComet: an
873 automated tool for comet assay image analysis. Redox Biol. 2014;2:457-65. Epub 20140109. doi:
874 10.1016/j.redox.2013.12.020. PubMed PMID: 24624335; PubMed Central PMCID: PMC3949099.
875 28. Allen KN, Dunaway-Mariano D. Markers of fitness in a successful enzyme superfamily.
876 Curr Opin Struct Biol. 2009;19(6):658-65. Epub 20091102. doi: 10.1016/j.sbi.2009.09.008.
877 PubMed PMID: 19889535; PubMed Central PMCID: PMC2787785.
878 29. Kuznetsova E, Nocek B, Brown G, Makarova KS, Flick R, Wolf YI, et al. Functional
879 Diversity of haloacid dehalogenase superfamily phosphatases from Saccharomyces cerevisiae:
880 Biochemical, structural, and evolutionary insights. J Biol Chem. 2015;290(30):18678-98. Epub
881 20150612. doi: 10.1074/jbc.M115.657916. PubMed PMID: 26071590; PubMed Central PMCID:
882 PMC4513125.
883 30. Langton M, Sun S, Ueda C, Markey M, Chen J, Paddy I, et al. The HD-Domain
884 Metalloprotein Superfamily: An Apparent Common Protein Scaffold with Diverse Chemistries.
885 Catalysts. 2020;10(10). Epub 20201015. doi: 10.3390/catal10101191. PubMed PMID: 34094591;
886 PubMed Central PMCID: PMC8177086.
887 31. Bianchi V, Spychala J. Mammalian 5'-nucleotidases. J Biol Chem. 2003;278(47):46195-8.
888 Epub 20030828. doi: 10.1074/jbc.R300032200. PubMed PMID: 12947102.
889 32. Wallden K, Ruzzenente B, Rinaldo-Matthis A, Bianchi V, Nordlund P. Structural basis for
890 substrate specificity of the human mitochondrial deoxyribonucleotidase. Structure.
891 2005;13(7):1081-8. doi: 10.1016/j.str.2005.04.023. PubMed PMID: 16004879.
892 33. Rampazzo C, Ferraro P, Pontarin G, Fabris S, Reichard P, Bianchi V. Mitochondrial
893 deoxyribonucleotides, pool sizes, synthesis, and regulation. J Biol Chem. 2004;279(17):17019-26.
894 Epub 20040126. doi: 10.1074/jbc.M313957200. PubMed PMID: 14747464.
895 34. de Saint Vincent BR, Dechamps M, Buttin G. The modulation of the thymidine
896 triphosphate pool of Chinese hamster cells by dCMP deaminase and UDP reductase. Thymidine
897 auxotrophy induced by CTP in dCMP deaminase-deficient lines. J Biol Chem. 1980;255(1):162-
898 7. PubMed PMID: 7350151.
899 35. Koharudin LM, Wu Y, DeLucia M, Mehrens J, Gronenborn AM, Ahn J. Structural basis
900 of allosteric activation of sterile alpha motif and histidine-aspartate domain-containing protein 1
901 (SAMHD1) by nucleoside triphosphates. J Biol Chem. 2014;289(47):32617-27. Epub 20141006.
902 doi: 10.1074/jbc.M114.591958. PubMed PMID: 25288794; PubMed Central PMCID:
903 PMC4239615.
904 36. Coggins SA, Mahboubi B, Schinazi RF, Kim B. SAMHD1 Functions and Human Diseases.
905 Viruses. 2020;12(4). Epub 20200331. doi: 10.3390/v12040382. PubMed PMID: 32244340;
906 PubMed Central PMCID: PMC7232136.
907 37. Yagüe-Capilla M, Castillo-Acosta VM, Bosch-Navarrete C, Ruiz-Pérez LM, González-
908 Pacanowska D. A Mitochondrial Orthologue of the dNTP Triphosphohydrolase SAMHD1 Is
909 Essential and Controls Pyrimidine Homeostasis in Trypanosoma brucei. ACS Infect Dis.
910 2021;7(2):318-32. doi: 10.1021/acsinfecdis.0c00551.
911 38. Henriksson S, Groth P, Gustafsson N, Helleday T. Distinct mechanistic responses to
912 replication fork stalling induced by either nucleotide or protein deprivation. Cell Cycle.

913 2018;17(5):568-79. Epub 20180402. doi: 10.1080/15384101.2017.1387696. PubMed PMID:
914 28976232; PubMed Central PMCID: PMC5969565.
915 39. Pu X, Wang Z, Klaunig JE. Alkaline Comet Assay for Assessing DNA Damage in
916 Individual Cells. Curr Protoc Toxicol. 2015;65:3 12 1-3 1. Epub 20150806. doi:
917 10.1002/0471140856.tx0312s65. PubMed PMID: 26250399.
918 40. Langie SA, Azqueta A, Collins AR. The comet assay: past, present, and future. Front Genet.
919 2015;6:266. Epub 20150813. doi: 10.3389/fgene.2015.00266. PubMed PMID: 26322077;
920 PubMed Central PMCID: PMC4534839.
921 41. Fernandes SA, Demetriades C. The Multifaceted Role of Nutrient Sensing and mTORC1
922 Signaling in Physiology and Aging. Front Aging. 2021;2:707372. Epub 20210827. doi:
923 10.3389/fragi.2021.707372. PubMed PMID: 35822019; PubMed Central PMCID: PMC9261424.
924 42. Takahara T, Amemiya Y, Sugiyama R, Maki M, Shibata H. Amino acid-dependent control
925 of mTORC1 signaling: a variety of regulatory modes. J Biomed Sci. 2020;27(1):87. Epub
926 20200817. doi: 10.1186/s12929-020-00679-2. PubMed PMID: 32799865; PubMed Central
927 PMCID: PMC7429791.
928 43. Vincent IM, Creek DJ, Burgess K, Woods DJ, Burchmore RJ, Barrett MP. Untargeted
929 metabolomics reveals a lack of synergy between nifurtimox and eflornithine against Trypanosoma
930 brucei. PLoS Negl Trop Dis. 2012;6(5):e1618. Epub 20120501. doi:
931 10.1371/journal.pntd.0001618. PubMed PMID: 22563508; PubMed Central PMCID:
932 PMC3341325.
933 44. Zoltner M, Campagnaro GD, Taleva G, Burrell A, Cerone M, Leung KF, et al. Suramin
934 exposure alters cellular metabolism and mitochondrial energy production in African trypanosomes.
935 J Biol Chem. 2020;295(24):8331-47. Epub 20200430. doi: 10.1074/jbc.RA120.012355. PubMed
936 PMID: 32354742; PubMed Central PMCID: PMC7294092.
937 45. Kumar V, Yadav S, Soumya N, Kumar R, Babu NK, Singh S. Biochemical and inhibition
938 studies of glutamine synthetase from Leishmania donovani. Microb Pathog. 2017;107:164-74.
939 Epub 20170325. doi: 10.1016/j.micpath.2017.03.024. PubMed PMID: 28351708.
940 46. Crispim M, Damasceno FS, Hernandez A, Barison MJ, Pretto Sauter I, Souza Pavani R, et
941 al. The glutamine synthetase of Trypanosoma cruzi is required for its resistance to ammonium
942 accumulation and evasion of the parasitophorous vacuole during host-cell infection. PLoS Negl
943 Trop Dis. 2018;12(1):e0006170. Epub 20180110. doi: 10.1371/journal.pntd.0006170. PubMed
944 PMID: 29320490; PubMed Central PMCID: PMC5779702.
945 47. de Jesus TC, Tonelli RR, Nardelli SC, da Silva Augusto L, Motta MC, Girard-Dias W, et
946 al. Target of rapamycin (TOR)-like 1 kinase is involved in the control of polyphosphate levels and
947 acidocalcisome maintenance in Trypanosoma brucei. J Biol Chem. 2010;285(31):24131-40. Epub
948 20100521. doi: 10.1074/jbc.M110.120212. PubMed PMID: 20495004; PubMed Central PMCID:
949 PMC2911323.
950 48. Barquilla A, Saldivia M, Diaz R, Bart JM, Vidal I, Calvo E, et al. Third target of rapamycin
951 complex negatively regulates development of quiescence in Trypanosoma brucei. Proc Natl Acad
952 Sci U S A. 2012;109(36):14399-404. Epub 20120820. doi: 10.1073/pnas.1210465109. PubMed
953 PMID: 22908264; PubMed Central PMCID: PMC3437835.
954 49. Barquilla A, Crespo JL, Navarro M. Rapamycin inhibits trypanosome cell growth by
955 preventing TOR complex 2 formation. Proc Natl Acad Sci U S A. 2008;105(38):14579-84. Epub
956 20080916. doi: 10.1073/pnas.0802668105. PubMed PMID: 18796613; PubMed Central PMCID:
957 PMC2567229.

958 50. Saldivia M, Barquilla A, Bart JM, Diaz-Gonzalez R, Hall MN, Navarro M. Target of
959 rapamycin (TOR) kinase in Trypanosoma brucei: an extended family. Biochem Soc Trans.
960 2013;41(4):934-8. doi: 10.1042/BST20130052. PubMed PMID: 23863159.
961 51. Parsons M, Worthey EA, Ward PN, Mottram JC. Comparative analysis of the kinomes of
962 three pathogenic trypanosomatids: Leishmania major, Trypanosoma brucei and Trypanosoma
963 cruzi. BMC Genomics. 2005;6:127. Epub 20050915. doi: 10.1186/1471-2164-6-127. PubMed
964 PMID: 16164760; PubMed Central PMCID: PMC1266030.
965 52. Proto WR, Coombs GH, Mottram JC. Cell death in parasitic protozoa: regulated or
966 incidental? Nat Rev Microbiol. 2013;11(1):58-66. Epub 20121203. doi: 10.1038/nrmicro2929.
967 PubMed PMID: 23202528.
968 53. Menna-Barreto RFS. Cell death pathways in pathogenic trypanosomatids: lessons of
969 (over)kill. Cell Death Dis. 2019;10(2):93. Epub 20190130. doi: 10.1038/s41419-019-1370-2.
970 PubMed PMID: 30700697; PubMed Central PMCID: PMC6353990.
971 54. Smirlis D, Duszenko M, Ruiz AJ, Scoulica E, Bastien P, Fasel N, et al. Targeting essential
972 pathways in trypanosomatids gives insights into protozoan mechanisms of cell death. Parasit
973 Vectors. 2010;3:107. Epub 20101117. doi: 10.1186/1756-3305-3-107. PubMed PMID: 21083891;
974 PubMed Central PMCID: PMC3136144.
975 55. Creek DJ, Nijagal B, Kim DH, Rojas F, Matthews KR, Barrett MP. Metabolomics guides
976 rational development of a simplified cell culture medium for drug screening against Trypanosoma
977 brucei. Antimicrob Agents Chemother. 2013;57(6):2768-79. Epub 20130409. doi:
978 10.1128/AAC.00044-13. PubMed PMID: 23571546; PubMed Central PMCID: PMC3716122.
979 56. Kim DH, Achcar F, Breitling R, Burgess KE, Barrett MP. LC-MS-based absolute
980 metabolite quantification: application to metabolic flux measurement in trypanosomes.
981 Metabolomics. 2015;11(6):1721-32. Epub 20150709. doi: 10.1007/s11306-015-0827-2. PubMed
982 PMID: 26491423; PubMed Central PMCID: PMC4605981.
983 57. Amos B, Aurrecoechea C, Barba M, Barreto A, Basenko EY, Bazant W, et al. VEuPathDB:
984 the eukaryotic pathogen, vector and host bioinformatics resource center. Nucleic Acids Res.
985 2022;50(D1):D898-D911. doi: 10.1093/nar/gkab929. PubMed PMID: 34718728; PubMed Central
986 PMCID: PMC8728164.
987 58. Shanmugasundram A, Starns D, Bohme U, Amos B, Wilkinson PA, Harb OS, et al.
988 TriTrypDB: An integrated functional genomics resource for kinetoplastida. PLoS Negl Trop Dis.
989 2023;17(1):e0011058. Epub 20230119. doi: 10.1371/journal.pntd.0011058. PubMed PMID:
990 36656904; PubMed Central PMCID: PMC9888696.
991 59. Booker ML, Bastos CM, Kramer ML, Barker RH, Jr., Skerlj R, Sidhu AB, et al. Novel
992 inhibitors of Plasmodium falciparum dihydroorotate dehydrogenase with anti-malarial activity in
993 the mouse model. J Biol Chem. 2010;285(43):33054-64. Epub 20100811. doi:
994 10.1074/jbc.M110.162081. PubMed PMID: 20702404; PubMed Central PMCID: PMC2963363.
995 60. Wirtz E, Leal S, Ochatt C, Cross GA. A tightly regulated inducible expression system for
996 conditional gene knock-outs and dominant-negative genetics in Trypanosoma brucei. Mol
997 Biochem Parasitol. 1999;99(1):89-101. doi: 10.1016/s0166-6851(99)00002-x. PubMed PMID:
998 10215027.
999 61. Li Q, Leija C, Rijo-Ferreira F, Chen J, Cestari I, Stuart K, et al. GMP synthase is essential
1000 for viability and infectivity of Trypanosoma bruceidespite a redundant purine salvage pathway.
1001 Mol Microbiol. 2015;97(5):1006-20.
1002 62. Xiao Y, Nguyen S, Kim SH, Volkov OA, Tu BP, Phillips MA. Product feedback regulation
1003 implicated in translational control of the Trypanosoma brucei S-adenosylmethionine

1004 decarboxylase regulatory subunit prozyme. Mol Microbiol. 2013;88(5):846-61. Epub 20130502.
1005 doi: 10.1111/mmi.12226. PubMed PMID: 23634831; PubMed Central PMCID: PMC3771639.
1006 63. Pfaffl MW. A new mathematical model for relative quantification in real-time RT-PCR.
1007 Nucleic Acids Res. 2001;29(9):e45. doi: 10.1093/nar/29.9.e45. PubMed PMID: 11328886;
1008 PubMed Central PMCID: PMC55695.
1009 64. Merritt C, Stuart K. Identification of essential and non-essential protein kinases by a fusion
1010 PCR method for efficient production of transgenic Trypanosoma brucei. Mol Biochem Parasitol.
1011 2013;190(1):44-9. Epub 20130516. doi: 10.1016/j.molbiopara.2013.05.002. PubMed PMID:
1012 23685343; PubMed Central PMCID: PMC3888357.
1013 65. Kim HS, Li Z, Boothroyd C, Cross GA. Strategies to construct null and conditional null
1014 Trypanosoma brucei mutants using Cre-recombinase and loxP. Mol Biochem Parasitol.
1015 2013;191(1):16-9. Epub 20130813. doi: 10.1016/j.molbiopara.2013.08.001. PubMed PMID:
1016 23954366; PubMed Central PMCID: PMC3830529.
1017 66. Scahill MD, Pastar I, Cross GA. CRE recombinase-based positive-negative selection
1018 systems for genetic manipulation in Trypanosoma brucei. Mol Biochem Parasitol. 2008;157(1):73-
1019 82. Epub 20071006. doi: 10.1016/j.molbiopara.2007.10.003. PubMed PMID: 18006158; PubMed
1020 Central PMCID: PMC2211722.
1021 67. Nguyen S, Jones DC, Wyllie S, Fairlamb AH, Phillips MA. Allosteric activation of
1022 trypanosomatid deoxyhypusine synthase by a catalytically dead paralog. J Biol Chem.
1023 2013;288(21):15256-67. Epub 20130321. doi: 10.1074/jbc.M113.461137. PubMed PMID:
1024 23525104; PubMed Central PMCID: PMC3663545.
1025 68. Wilson PM, Labonte MJ, Russell J, Louie S, Ghobrial AA, Ladner RD. A novel
1026 fluorescence-based assay for the rapid detection and quantification of cellular deoxyribonucleoside
1027 triphosphates. Nucleic Acids Res. 2011;39(17):e112. doi: 10.1093/nar/gkr350. PubMed Central
1028 PMCID: PMC3177181.
1029 69. Pontikos MA, Leija C, Zhao Z, Wang X, Kilgore J, Tornesi B, et al. Development of a
1030 biomarker to monitor target engagement after treatment with dihydroorotate dehydrogenase
1031 inhibitors. Biochem Pharmacol. 2022;204:115237. Epub 20220831. doi:
1032 10.1016/j.bcp.2022.115237. PubMed PMID: 36055381; PubMed Central PMCID: PMC9547971.
1033 70. Su X, Li X, Wang H, Cai Z. Simultaneous determination of methionine cycle metabolites,
1034 urea cycle intermediates and polyamines in serum, urine and intestinal tissue by using UHPLC-
1035 MS/MS. Talanta. 2021;224:121868. Epub 20201105. doi: 10.1016/j.talanta.2020.121868.
1036 PubMed PMID: 33379078.
1037 71. Lorkiewicz PK, Gibb AA, Rood BR, He L, Zheng Y, Clem BF, et al. Integration of flux
1038 measurements and pharmacological controls to optimize stable isotope-resolved metabolomics
1039 workflows and interpretation. Sci Rep. 2019;9(1):13705. Epub 20190923. doi: 10.1038/s41598-
1040 019-50183-3. PubMed PMID: 31548575; PubMed Central PMCID: PMC6757038.
1041 72. Wyllie S, Foth BJ, Kelner A, Sokolova AY, Berriman M, Fairlamb AH. Nitroheterocyclic
1042 drug resistance mechanisms in Trypanosoma brucei. J Antimicrob Chemother. 2016;71(3):625-34.
1043 Epub 20151117. doi: 10.1093/jac/dkv376. PubMed PMID: 26581221; PubMed Central PMCID:
1044 PMC4743696.
1045 73. Sokolova AY, Wyllie S, Patterson S, Oza SL, Read KD, Fairlamb AH. Cross-resistance to
1046 nitro drugs and implications for treatment of human African trypanosomiasis. Antimicrob Agents
1047 Chemother. 2010;54(7):2893-900. Epub 20100503. doi: 10.1128/AAC.00332-10. PubMed PMID:
1048 20439607; PubMed Central PMCID: PMC2897277.
1049

1050 **Figure Captions**

1051 **Fig 1. Pyrimidine biosynthesis pathway in *T. brucei*.**

1052 Green indicates *de novo* pathway metabolites, and red represents the main salvaged metabolite
1053 uracil. The reaction catalyzed by human DCTD, which is used to rescue TK and 5'-HDNT
1054 knockouts, is indicated with a dashed red line. Enzyme abbreviations above each arrow are as
1055 follows: CPS carbamoyl phosphate synthase; ATCase aspartate carbamoyl transferase; DHOase
1056 dihydroorotase; DHODH dihydroorotate dehydrogenase; UMPS uridine monophosphate synthase;
1057 CMPK UMP-CMP kinase; NDPK nucleoside diphosphate kinase; CTPS cytidine triphosphate
1058 synthase; DHFR-TS dihydrofolate reductase-thymidylate synthase; TMPK thymidylate kinase;
1059 RNR ribonucleotide reductase; DCTD human dCMP deaminase – dashed line indicates this gene
1060 is not encoded by *T. brucei*; CDA cytidine deaminase; UPase uridine phosphorylase; UPRT uracil
1061 phosphoribosyltransferase; TK thymidine kinase; 5'-HDNT HD domain 5'-nucleotidase; HAD2
1062 haloacid dehalogenase-like 5'-nucleotidase. Non-nucleotide abbreviations are as follows: DHO
1063 dihydroorotate; Ctd cytidine; Urd uridine; dThd thymidine; dCtd 2'-deoxycytidine; dUrd 2'-
1064 deoxyuridine.

1065

1066 **Fig 2. Substrate and metal ion dependance of *T. brucei* 5'-nucleotidases.**

1067 (A-C) Metal ion dependence of 5'-HDNT (A), HAD1 (B), and HAD2 (C) showing specific activity
1068 under the indicated conditions. Substrates were dCMP (1 mM) for 5'-HDNT, CTP (1 mM) for
1069 HAD1, and dTMP (1 mM) for HAD2. (D-F) Substrate specificity of 5'-HDNT (D), HAD1 (E),
1070 and HAD2 (F) showing k_{cat}/K_M for the indicated substrates. Individual kinetic constants can be
1071 found in S1 Table. Activity assays included the following metal ions: Co^{2+} (0.5 mM) for 5'-HDNT,
1072 Mg^{2+} (5 mM) for HAD1, and Mg^{2+} (5 mM) for HAD2. The < symbol indicates activity was below

1073 the level of detection. Data represent biological triplicates based on 3 technical replicates per
1074 substrate concentration, and error bars show the standard deviation (SD).
1075
1076 **Fig 3. 5'-HDNT is essential in *T. brucei* and is functionally rescued by *Hs*DCTD.**
1077 (A and D) Growth curves of 5'-HDNT c-null cells expressing either FLAG-tagged *Tb*5'-HDNT
1078 (5'-HDNT$^{-/-}$Tet(5'-HDNT)) (blue) or *Hs*DCTD (5'-HDNT$^{-/-}$Tet(*Hs*DCTD)) (green) under Tet
1079 regulation. Cell growth was monitored ±Tet in FBS (A) or dFBS (D) for the days indicated. (B
1080 and E) qPCR analysis of relative mRNA expression of *Tb*5'-HDNT or *Hs*DCTD ±Tet in FBS (B)
1081 or dFBS (E). (C and F) Relative protein expression of 5'-HDNT (blue) or *Hs*DCTD (green) ±Tet
1082 in FBS (C) or dFBS (F). Protein expression levels were determined using a capillary-based
1083 Western immunoassay (ProteinSimple Jess). Protein expression was normalized to Hsp70 as a
1084 loading control. Representative digital Western blot images for panels (C) and (F) are shown in
1085 S4A Fig and S4B Fig, respectively. For all panels, data represent triplicate biological replicates,
1086 and error bars show the SD.
1087
1088 **Fig 4. Metabolomic analysis of 5'-HDNT c-null cell lines.**
1089 Volcano plot representation of metabolite differences between –Tet and +Tet conditions of 5'-
1090 HDNT c-null cells expressing 5'-HDNT (A) or *Hs*DCTD (B) 48 h after Tet removal. Pyrimidine
1091 pathway metabolites that are significantly decreased are shown in blue, those that are significantly
1092 increased are in red, and those that are not significantly impacted are shown in black. The dotted
1093 horizontal line represents the statistical significance threshold ($p < 0.05$), and the dotted vertical
1094 lines mark thresholds of $\log_2$ (fold change) >1 and < -1. Data represent one experiment with 3
1095 technical replicates. Two additional biological replicates are shown in S6 Fig. Identity of blue, red,

1096 and black metabolites are annotated in S3 Table. Non-nucleotide abbreviations: CP carbamoyl
1097 phosphate; CDP-Etn CDP-ethanolamine; CDP-Cho CDP-choline; Gln glutamine; UDP-GlcNAc
1098 UDP-N-acetylglucosamine.
1099
1100 **Fig 5. dNTP levels in 5'-HDNT c-null cells.**
1101 (A) Quantitation of nucleotide levels by polymerase-based fluorescence assay in 5'-HDNT c-null
1102 cells grown with and without Tet for 48 h. Inset shows mRNA expression of *Tb*5'-HDNT in
1103 response to Tet. Data represent the total of n=4 independent experiments, each derived from 3
1104 technical triplicates, and error bars show the SD. The full data sets for each independent replicate
1105 are shown in S5 Table. (B) dNTP ratios in 5'-HDNT c-null cells ±Tet for 48 h. Data represent the
1106 same experiment as in (A), and error bars show the SD. Dotted line indicates a nucleotide ratio of
1107 1. Student's t-test analysis was performed for both panels with significant differences between
1108 +Tet and –Tet marked as follows: *$p < 0.05$, **$p < 0.005$.
1109
1110 **Fig 6. Thymidine kinase and 5'-HDNT double knockout is lethal in *T. brucei*.**
1111 (A) Growth analysis of TK and 5'-HDNT double knockout in normal (FBS) and dialyzed (dFBS)
1112 serum. The ~ symbol indicates only cell debris remained. Log 4 is the limit of detection of the
1113 assay. (B) qPCR analysis of *Tb*TK and *Tb*5'-HDNT mRNA expression ±Tet for 48 h in the TK/5'-
1114 HDNT double knockout cell line. (C) Relative protein expression of TK and 5'-HDNT ±Tet for
1115 48 h normalized to Hsp70 as a loading control. Protein expression was collected using a capillary-
1116 based Western immunoassay (ProteinSimple Jess). Representative digital Western blot image is
1117 shown in S4C Fig. Data represent triplicate biological replicates, and error bars show the SD. The
1118 < symbol indicates expression was not detected. (D and E) Metabolomic analysis of TK/5'-HDNT

1119 double knockout cell line. Volcano plot representation of metabolite differences between –Tet and
1120 +Tet conditions of TK/5'-HDNT c-null cells grown in normal (D) or dialyzed (E) serum. Blue
1121 represents metabolites in the pyrimidine biosynthesis pathway. Dotted horizontal line represents
1122 the statistical significance threshold ($p < 0.05$), and the dotted vertical lines mark thresholds of
1123 $\log_2$ (fold change) >1 and < -1. Metabolite data represent one experiment with 3 technical replicates.
1124 The full metabolite data set can be found in S7 Table. Abbreviations are as described in Fig 4.
1125

1126 **Fig 7. L-Gln uptake in 5'-HDNT c-null cells.**

1127 (A) mRNA expression of *Tb*5'-HDNT ±Tet for 48 h in the 5'-HDNT$^{-/-}$Tet(5'-HDNT) cells used
1128 to determine L-Gln uptake. (B-D) Uptake of $^{13}C_5{}^{15}N_2$ L-Gln showing pmoles/10^6 cells
1129 incorporated (B) and detection of labeled glutamate (C) and labeled succinate (D) in 5'-HDNT c-
1130 null cells 48 h after Tet removal. Data in panels C and D are plotted as the % isotopically labeled
1131 metabolite incorporated as a fraction of the total, including both labeled and unlabeled, uncorrected
1132 for natural isotope abundance. (E) Uptake of $^{13}C_5$ L-ornithine in 5'-HDNT c-null cells 48 h after
1133 Tet removal shown as % incorporation of labeled L-Orn versus total of labeled and unlabeled L-
1134 Orn pools in the cell. Data represent duplicate biological replicates based on 1-2 technical
1135 replicates for each, and error bars show the SD. Additional biological replicates showing $^{13}C_5{}^{15}N_2$
1136 L-Gln uptake are shown in S9 Fig.
1137

1138 **Fig 8. PCR-based detection of DNA lesions in 5'-HDNT c-null cells.**

1139 (A) DNA lesions detected per 10 kb in wild-type SM or 5'-HDNT knockout cells. (B) Growth of
1140 5'-HDNT c-null cells following treatment with DNA damaging compounds or Tet removal for the
1141 indicated times. All other cells were grown for 48 h. Cells were treated with HU (100 μM) and

1142 MMS (0.002%) for 24 h prior to harvesting. $5x10^7$ cells were harvested per condition. (C) DNA
1143 lesions per 10 kb in wild-type SM *T. brucei* nuclear DNA 48 h after drug treatment. (D) Growth
1144 of wild-type cells 48 h after treatment with indicated compounds. For (C) and (D), cells were
1145 treated according to published EC_{50} values: eflornithine 15 μM, pentamidine 2.5 nM, suramin 27
1146 nM (all from [26]), fexinidazole 1 μM [72, 73]. NT represents non-treated cells. Data represent
1147 triplicate biological replicates from 3 technical replicates each, and error bars show the SD.
1148

1149 **Fig 9. DNA comet assay-based detection of DNA damage in 5'-HDNT c-null cells.**
1150 (A) Representative fluorescence images of wild-type and 5'-HDNT c-null cells displaying the
1151 median tail moments for each condition (as calculated in Fig 9B). SM wild-type and 5'-HDNT c-
1152 null cells ±Tet were grown for 48 h, and positive control cells were treated with MMS (0.002%)
1153 for 24 h prior to assay. (B) Plot of tail moments of 50 comets per sample analyzed by OpenComet
1154 v1.3.1. Error bars represent the standard error of the mean (SEM). Data were analyzed by one-way
1155 ANOVA with Šidák correction for multiple comparisons. Significant differences between
1156 conditions are marked as shown: ****$p < 0.0001$. Two additional biological replicates are reported
1157 in S11 Fig. (C) qPCR analysis of *Tb*5'-HDNT mRNA expression ±Tet. Data represent triplicate
1158 biological replicates, and error bars show the SD. (D) Relative protein expression of 5'-HDNT
1159 ±Tet normalized to Hsp70. Representative digital Western blot image is shown in S4D Fig.
1160

1161 **Fig 10. Model of cell death in 5'-HDNT null cells.**
1162 In this model, loss of 5'-HDNT prevents interconversion between nucleotides and nucleosides,
1163 particularly the recycling of C nucleotides. Nucleotide imbalance causes damage to nuclear DNA,

1164 leading to downregulation of L-Gln uptake through an unknown signaling mechanism, eventually

1165 resulting in cell death.

1166 **Supporting Information Captions**

1167 **S1 Fig. Amino acid alignment of HAD domain proteins from select species.**

1168 HAD domain proteins from *T. brucei* (*T.b. brucei*: XP_827334.1; *T.b. gambiense*:
1169 XP_011776801.1), *Leishmania* (*L. donovani*: CAC5434461.1; *L. tarentole*: GET92950.1), *T. cruzi*
1170 (*T. cruzi*: RNF19517.1; *T.c. marinkellei*: EKF31807.1), *Escherichia coli* (HAD: PPI92248.1;
1171 NagD: P0AF24.1), *Saccharomyces cerevisiae* (3RF6), *Candida albicans* (KGQ98905.1), *Mus*
1172 *musculus* (NP_659064.1), and *Homo sapiens* (NP_060299.4). Red sequence indicates *T. brucei*
1173 HAD2. Residue highlighted in yellow indicates the starting amino acid of HAD2 N-terminal
1174 truncation (HAD2_Δ1-136).

1175

1176 **S2 Fig. Non-essential HAD domain nucleotidases.**

1177 Growth analysis of HAD domain nucleotidase HAD1 null (A) and HAD2 null (D) cells in normal
1178 (FBS) and dialyzed (dFBS) serum. qPCR analysis of relative mRNA expression of *Tb*HAD1 and
1179 *Tb*HAD2 compared to wild type cells shown in (B) and (E) respectively. Data represent triplicate
1180 biological replicates each based on 3 technical replicates, and error bars show the SD. Metabolite
1181 analysis of HAD1 knockout cells (C) and HAD2 knockout cells (F) compared to wild type cells
1182 with pyrimidine metabolites shown in blue. Identity of blue metabolites is annotated in S6 Table.
1183 Both experiments were collected in FBS. Metabolite data represent one experiment with 3
1184 technical replicates.

1185

1186 **S3 Fig. 5'-HDNT is essential for growth in *T. brucei*.**

1187 These data represent an extra set of independent experiments to those described in Fig 3 for the
1188 5'-HDNT knockdown cells. (A) Growth analysis of 5'-HDNT knockout in normal (FBS) and

1189 dialyzed (dFBS) serum. Inset: Western blot of FLAG-tagged 5'-HDNT under Tet regulation and
1190 Hsp70 as a loading control. (B) qPCR analysis of relative mRNA expression of *Tb*5'-HDNT ±Tet
1191 for 24 h with *TERT* as a reference gene. Growth curve and PCR data represent triplicate biological
1192 replicates, and error bars show the SD. The inset Western blot is a single representative example
1193 for one of the three studies in this figure.
1194
1195 **S4 Fig. Representative digital Western blot images of FLAG-tagged *Tb*5'-HDNT, *Hs*DCTD,**
1196 **and *Tb*TK protein expression in response to Tet.**
1197 (A and B) Expression of either 5'-HDNT (A) or *Hs*DCTD (B) in 5'-HDNT c-null cells as described
1198 in Fig 3. (C) Tet-regulated expression of TK and 5'-HDNT in the TK/5'-HDNT DKO cell line
1199 described in Fig 6. (D) Expression of 5'-HDNT ±Tet for the experiment described in Fig 9. Protein
1200 expression is normalized to total protein (TP) measurements shown in blue, with lane 2 serving as
1201 the reference lane. (E) Expression of 5'-HDNT ±Tet for the experiment described in S9 Fig,
1202 normalized to total protein measurements in each capillary (blue dots). Digital Western blot images
1203 generated by Compass for SW software v5.0.1 (ProteinSimple). Bands corresponding to loading
1204 control Hsp70 (70 kDa), FLAG-tagged TK (53 kDa), *Hs*DCTD (30 kDa), and 5'-HDNT (28 kDa)
1205 are indicated. NS (48 kDa) marks a nonspecific band.
1206
1207 **S5 Fig. Pyrimidine supplementation fails to rescue 5'-HDNT knockout.**
1208 Growth curves of 5'-HDNT c-null cells grown in dFBS and supplemented with 250 μM or 500
1209 μM Thd (A), 2 mM or 5 mM dUrd (B), 1 mM dCtd (C), 1 mM Urd (D), 1 mM Ctd (E), and 100
1210 μM uracil (F). 5'-HDNT c-null cells express an ectopic copy of Tet-regulated *Tb*5'-HDNT, and

1211 mRNA expression of *Tb*5'-HDNT 48 h after Tet removal is shown to the right of each panel. All
1212 error bars represent SD for triplicate biological data.
1213
1214 **S6 Fig. Metabolomic analysis of 5'-HDNT c-null cells expressing *Tb*5'-HDNT (A and B) or**
1215 ***Hs*DCTD (D and E) as described in Fig 4.**
1216 Volcano plots show metabolites that are significantly different between –Tet and +Tet cells after
1217 48 h. Blue shows significantly changed pyrimidine metabolites, black shows other pyrimidine
1218 metabolites, and red represents the metabolite dCMP. Each panel is derived from 3 technical
1219 replicates, with panels (A) and (B), and (D) and (E), representing additional biological replicates
1220 of the data shown in Fig 4. Identity of blue, red, and black metabolites are annotated in S3 Table.
1221 Abbreviations are as described in Fig 4. Dotted horizontal line represents the statistical
1222 significance threshold ($p < 0.05$), and the dotted vertical lines mark thresholds of $\log_2$ (fold
1223 change) >1 and < -1. (C and F) Relative mRNA expression of *Tb*5'-HDNT (C) or *Hs*DCTD (F)
1224 ±Tet in cells used for metabolomics analysis as described in Fig 4 and S6 Fig. Data represent
1225 triplicate biological replicates, and error bars show the SD.
1226
1227 **S7 Fig. Fold change ratios of pyrimidine metabolites detected in 5'-HDNT c-null cells**
1228 **expressing *Tb*5'-HDNT (A) or *Hs*DCTD (B) 48 h after Tet removal as described in Fig 4.**
1229 Each panel plots the mean fold change of three biological replicates as shown in Fig 4 of main text
1230 and S6 Fig. Error bars show the SD. Individual fold change values are reported in S4 Table. Some
1231 metabolites were detected using multiple chromatography techniques (see Materials and Methods)
1232 and are indicated with the following: _1 C18 reversed phase column, _2 pHILIC column.
1233

1234 **S8 Fig. PCR and qPCR analysis of TK/5'-HDNT DKO cell line.**

1235 (A) *Tb*TK and *Tb*5'-HDNT were amplified from genomic DNA extracted from TK/5'-HDNT
1236 DKO cells and SM wild-type cells. The selectable markers were amplified from TK/5'-HDNT
1237 DKO genomic DNA. (B) qPCR analysis of mRNA expression of *Tb*5'-HDNT or *Tb*TK ±Tet for
1238 24 h with *TERT* as a reference gene in the cells used for metabolomics analysis as described in Fig
1239 6. Data represent triplicate technical replicates, and error bars show the SEM.

1240

1241 **S9 Fig. Uptake of L-Gln in 5'-HDNT c-null cells.**

1242 Uptake of $^{13}C_5{}^{15}N_2$ L-Gln (A) and detection of labeled glutamate (B), labeled succinate (C), and
1243 labeled UMP (D) in 5'-HDNT c-null cells 48 h after Tet removal. Data are plotted as the %
1244 isotopically labeled metabolite incorporated as a fraction of the total including both labeled and
1245 unlabeled, uncorrected for natural isotope abundance. Data represent duplicate biological
1246 replicates based on 2 technical replicates for each, and error bars show the SD. Panels A-C
1247 represent data from the same experiment. Panel D is a separate experiment. 5'-HDNT protein
1248 levels were assessed to confirm knockdown in the cells used for these studies, and data are shown
1249 in S4E Fig. See Fig 7 for additional experimental details.

1250

1251 **S10 Fig. Representative chromatograms for glutamine, glutamate, succinate, UMP, and**
1252 **ornithine in isotope uptake assays.** (A-D) Chromatograms of glutamine (*m*/*z* 145 → *m*/*z* 127)
1253 and $^{13}C_5{}^{15}N_2$ glutamine (*m*/*z* 152 → *m*/*z* 134). (E-H) Chromatograms of glutamate (*m*/*z* 146 → *m*/*z*
1254 128) and $^{13}C_5{}^{15}N_1$ glutamate: (*m*/*z* 152 → *m*/*z* 134). Identical transition was used for $^{13}C_5{}^{15}N_2$
1255 glutamine and $^{13}C_5{}^{15}N_1$ glutamate. Peak identity was verified by matching retention times with the
1256 unlabeled metabolite. (I-L) Chromatograms of succinate (*m*/*z* 117 → *m*/*z* 99) and $^{13}C_4$ succinate

1257 (*m/z* 121 → *m/z* 103). (M-P) Chromatograms of UMP (*m/z* 325.1 → *m/z* 97) and UMP M+1 (*m/z*
1258 326.1 → *m/z* 97). (Q-T) Chromatograms for ornithine (*m/z* 133 → *m/z* 70) and $^{13}C_5$ ornithine (*m/z*
1259 138.1 → *m/z* 74.2). Chromatograms represent the 15 min assay timepoint for UMP and 60 sec
1260 timepoint for all other metabolites. For all panels, retention time (RT) and Tet treatment are as
1261 indicated, and the shaded region represents metabolite peak area.
1262
1263 **S11 Fig. Tail moments of wild type and 5'-HDNT c-null cells as measured by the Comet assay.**
1264 50 comets were analyzed per condition with the mean indicated. Error bars show the SEM. (A)
1265 and (B) are separate biological replicates. Conditions are as described in Fig 9. Data were analyzed
1266 by one-way ANOVA with Šidák correction for multiple comparisons. Significant differences
1267 between conditions are marked as shown: ****$p < 0.0001$.
1268
1269 **S1 Table. *T. brucei* 5'-nucleotidase steady-state kinetic constants**
1270 **S2 Table. List of *T. brucei* genetically engineered cell lines**
1271 **S3 Table. Metabolomic analysis of 5'-HDNT c-null cells**
1272 **S4 Table. Fold change of metabolites in 5'-HDNT c-null cells**
1273 **S5 Table. Quantitation of dNTP levels in 5'-HDNT c-null cells**
1274 **S6 Table. Metabolomic analysis of HAD1 and HAD2 null cells**
1275 **S7 Table. Metabolomic analysis of TK/5'-HDNT c-null cells**
1276 **S8 Table. Primers**
1277

Fig 1

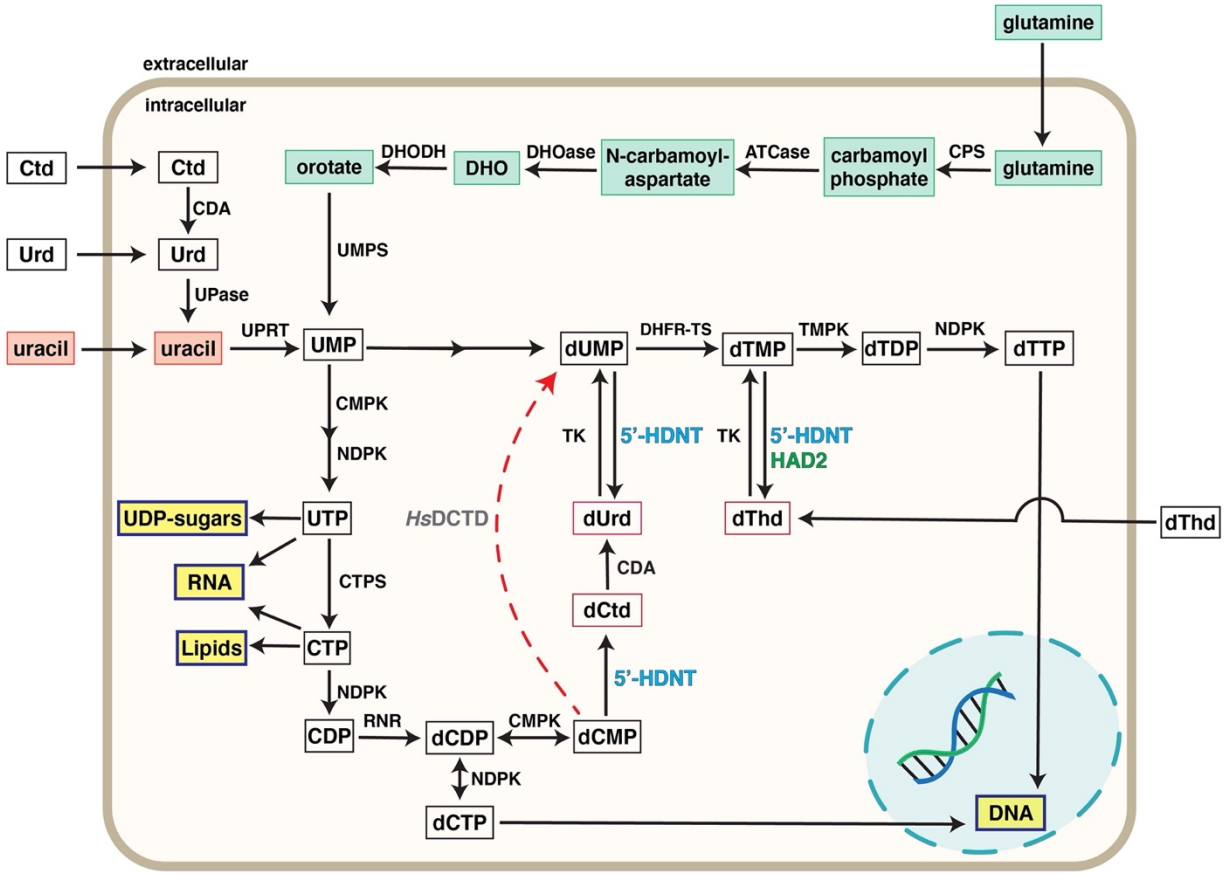
glutamine
extracellular
intracellular
Ctd
Ctd
CDA
Urd
Urd
UPase
uracil
uracil
UPRT
orotate
DHODH
DHO
DHOase
N-carbamoyl-aspartate
ATCase
carbamoyl phosphate
CPS
glutamine
UMPS
UMP
dUMP
DHFR-TS
dTMP
TMPK
dTDP
NDPK
dTTP
CMPK
NDPK
TK
5'-HDNT
TK
5'-HDNT
HAD2
UDP-sugars
UTP
HsDCTD
dUrd
dThd
dThd
RNA
CTPS
CDA
dCtd
Lipids
CTP
5'-HDNT
NDPK
CDP
RNR
dCDP
CMPK
dCMP
NDPK
dCTP
DNA

Fig 2

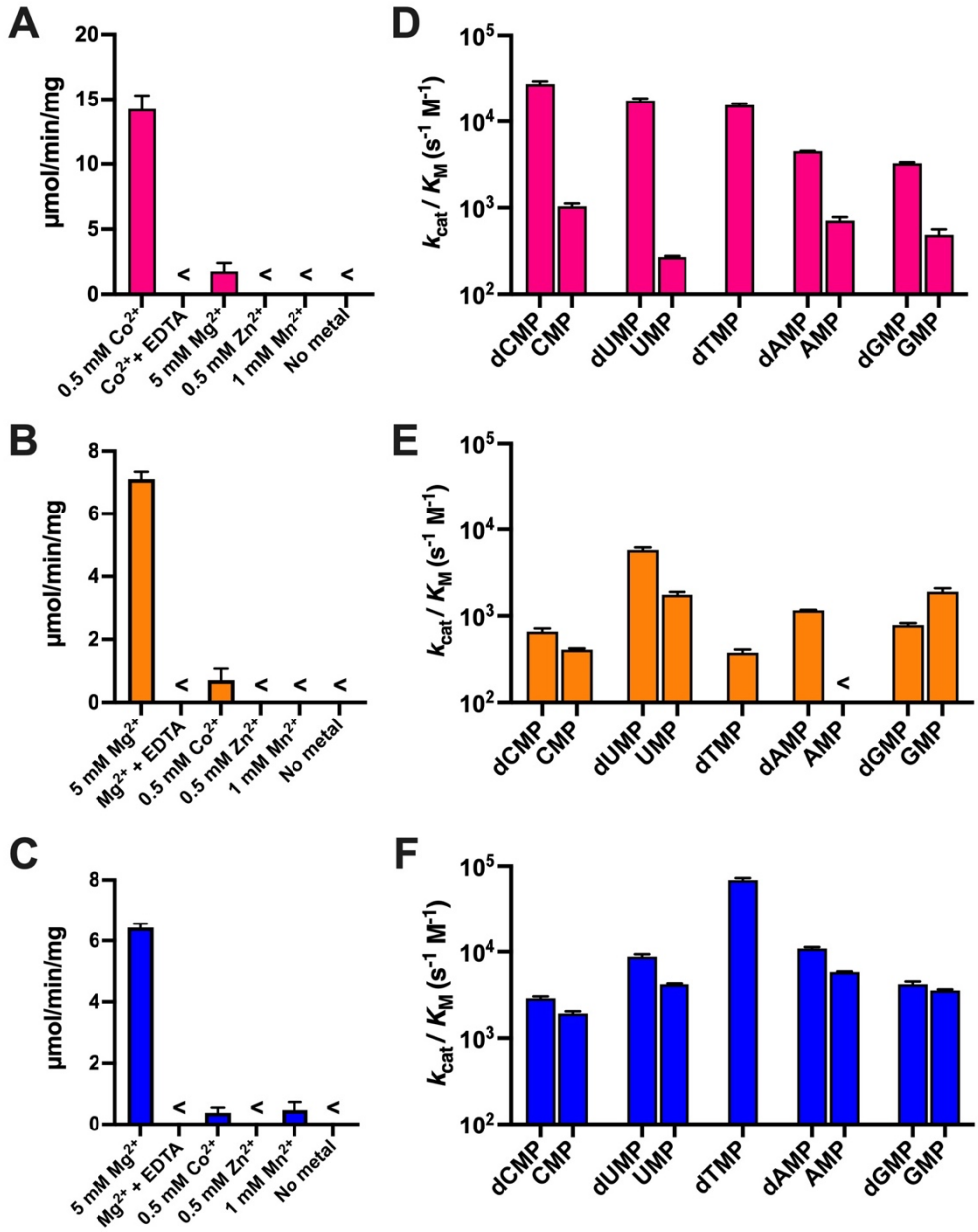
A
B
C
D
E
F
μmol/min/mg
k_{cat} / K_M (s^{-1} M^{-1})
0.5 mM Co^{2+}
Co^{2+} + EDTA
5 mM Mg^{2+}
0.5 mM Zn^{2+}
1 mM Mn^{2+}
No metal
Mg^{2+} + EDTA
dCMP
CMP
dUMP
UMP
dTMP
dAMP
AMP
dGMP
GMP

Fig 3

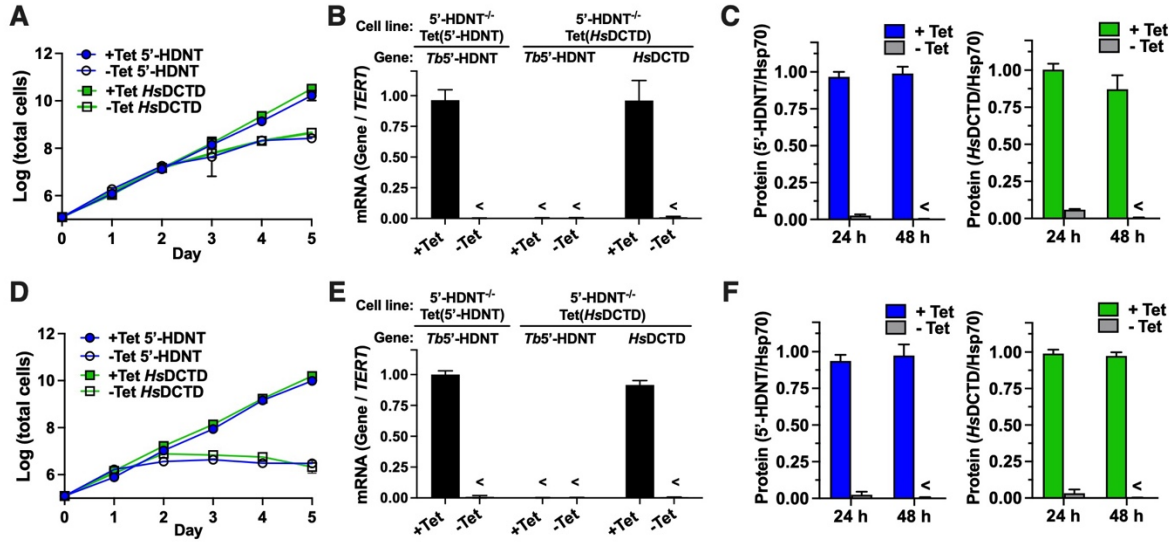
A
+Tet 5'-HDNT
-Tet 5'-HDNT
+Tet HsDCTD
-Tet HsDCTD
Log (total cells)
Day
B
Cell line:
5'-HDNT-/- Tet(5'-HDNT)
5'-HDNT-/- Tet(HsDCTD)
Gene:
Tb5'-HDNT
Tb5'-HDNT
HsDCTD
mRNA (Gene / TERT)
+Tet
-Tet
C
+ Tet
- Tet
Protein (5'-HDNT/Hsp70)
Protein (HsDCTD/Hsp70)
24 h
48 h
D
E
F

Fig 4

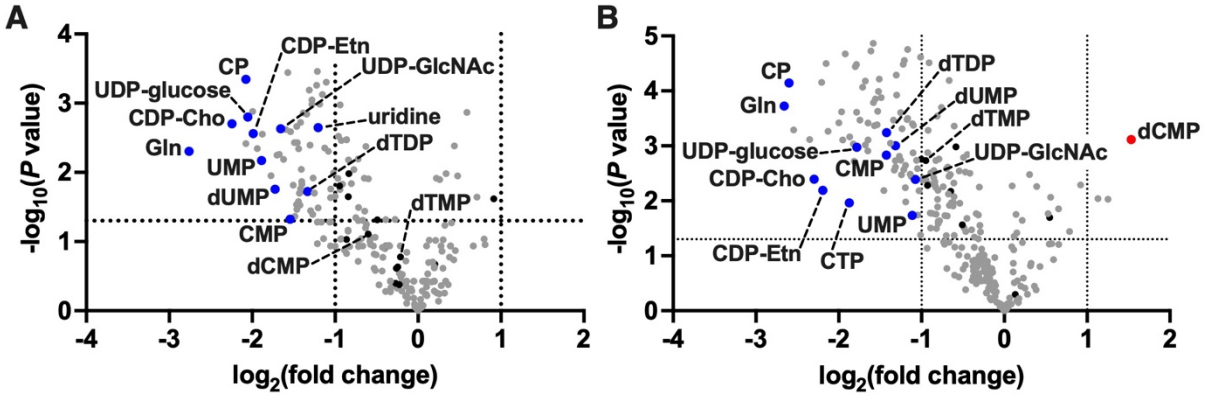
A
CDP-Etn
CP
UDP-GlcNAc
UDP-glucose
CDP-Cho
uridine
Gln
dTDP
UMP
dUMP
dTMP
CMP
dCMP
-log10(P value)
log2(fold change)
B
CP
dTDP
Gln
dUMP
dTMP
dCMP
UDP-glucose
UDP-GlcNAc
CDP-Cho
CMP
UMP
CDP-Etn
CTP
-log10(P value)
log2(fold change)

Fig 5

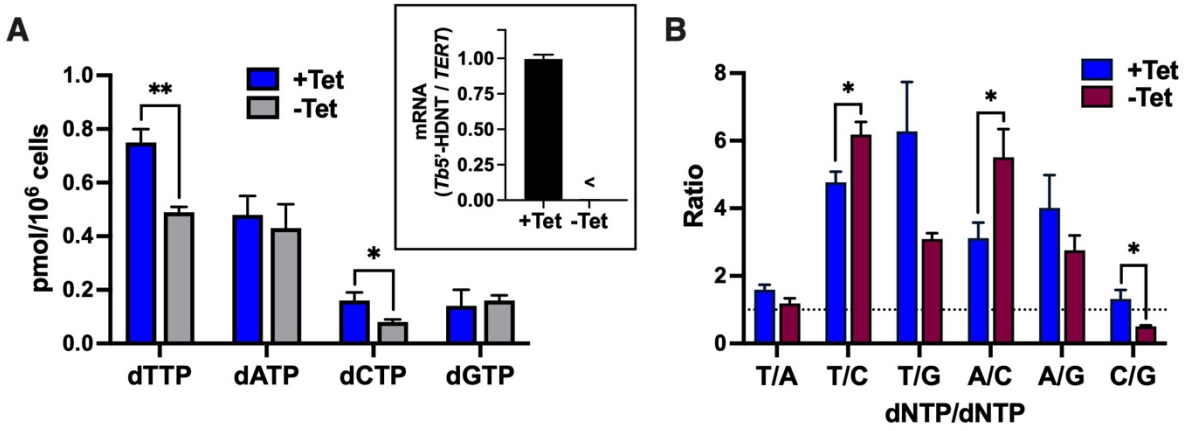
A
pmol/10^6 cells
1.0
0.8
0.6
0.4
0.2
0.0
**
*
+Tet
-Tet
dTTP
dATP
dCTP
dGTP
mRNA
(Tb5'-HDNT / TERT)
1.00
0.75
0.50
0.25
0.00
<
+Tet
-Tet
B
Ratio
8
6
4
2
0
*
*
*
+Tet
-Tet
T/A
T/C
T/G
A/C
A/G
C/G
dNTP/dNTP

Fig 6

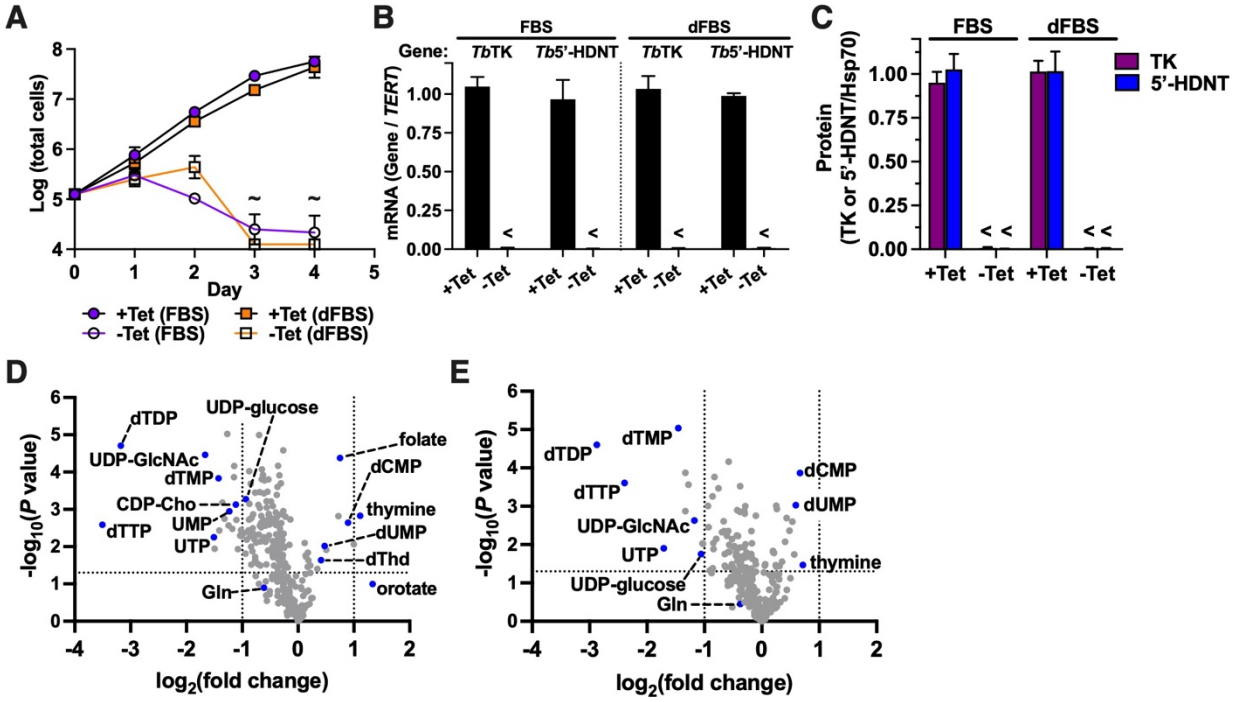
A
Log (total cells)
Day
+Tet (FBS)
-Tet (FBS)
+Tet (dFBS)
-Tet (dFBS)
B
FBS
dFBS
Gene:
TbTK
Tb5'-HDNT
mRNA (Gene / TERT)
+Tet
-Tet
C
Protein (TK or 5'-HDNT/Hsp70)
TK
5'-HDNT
D
-log10(P value)
log2(fold change)
dTDP
UDP-glucose
UDP-GlcNAc
dTMP
CDP-Cho
dTTP
UMP
UTP
Gln
folate
dCMP
thymine
dUMP
dThd
orotate
E
dTDP
dTMP
dTTP
UDP-GlcNAc
UTP
UDP-glucose
Gln
dCMP
dUMP
thymine

Fig 7

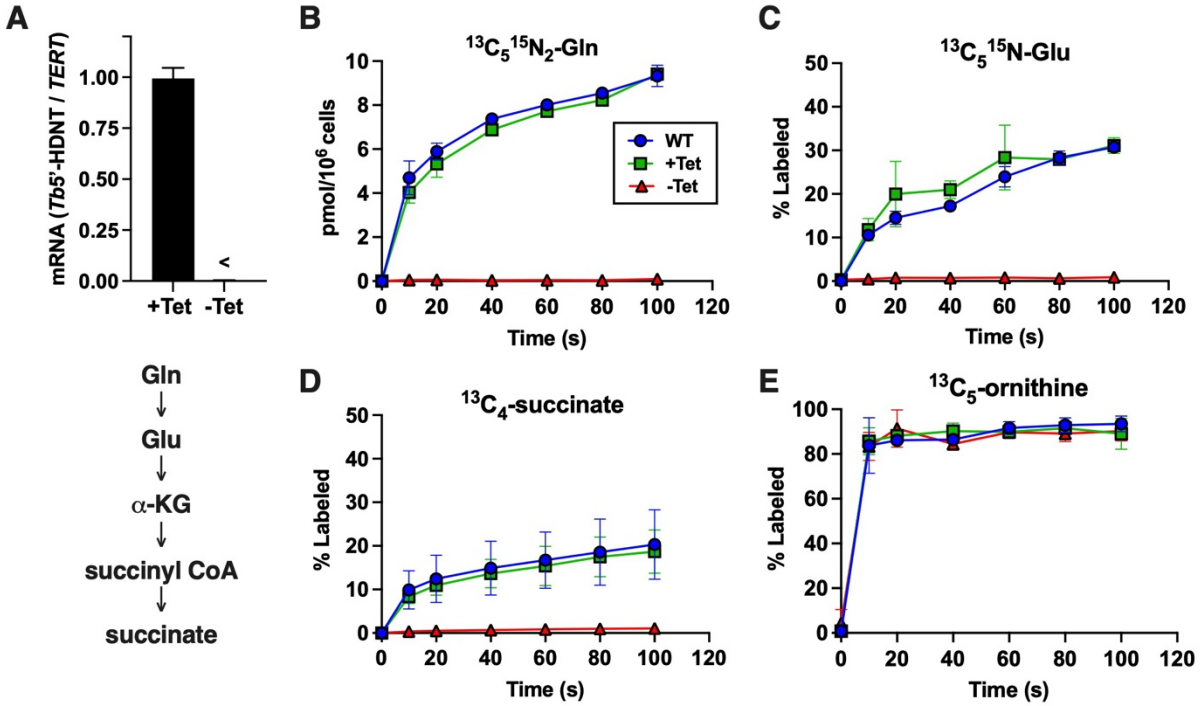
A
mRNA (Tb5'-HDNT / TERT)
1.00
0.75
0.50
0.25
0.00
<
+Tet
-Tet
B
$^{13}C_5{}^{15}N_2$-Gln
pmol/10^6 cells
WT
+Tet
-Tet
Time (s)
C
$^{13}C_5{}^{15}N$-Glu
% Labeled
Time (s)
Gln
Glu
α-KG
succinyl CoA
succinate
D
$^{13}C_4$-succinate
% Labeled
Time (s)
E
$^{13}C_5$-ornithine
% Labeled
Time (s)

Fig 8

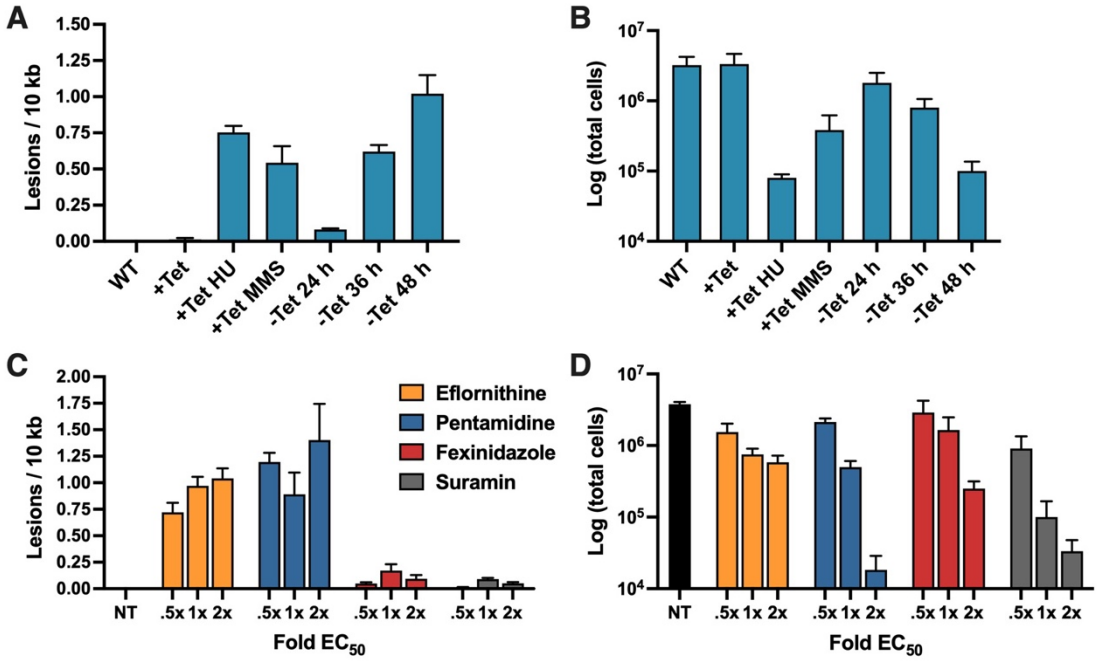
A
Lesions / 10 kb
1.50
1.25
1.00
0.75
0.50
0.25
0.00
WT
+Tet
+Tet HU
+Tet MMS
-Tet 24 h
-Tet 36 h
-Tet 48 h
B
Log (total cells)
10^7
10^6
10^5
10^4
WT
+Tet
+Tet HU
+Tet MMS
-Tet 24 h
-Tet 36 h
-Tet 48 h
C
Lesions / 10 kb
2.00
1.75
1.50
1.25
1.00
0.75
0.50
0.25
0.00
Eflornithine
Pentamidine
Fexinidazole
Suramin
NT
.5x 1x 2x
.5x 1x 2x
.5x 1x 2x
.5x 1x 2x
Fold EC_{50}
D
Log (total cells)
10^7
10^6
10^5
10^4
NT
.5x 1x 2x
.5x 1x 2x
.5x 1x 2x
.5x 1x 2x
Fold EC_{50}

Fig 9

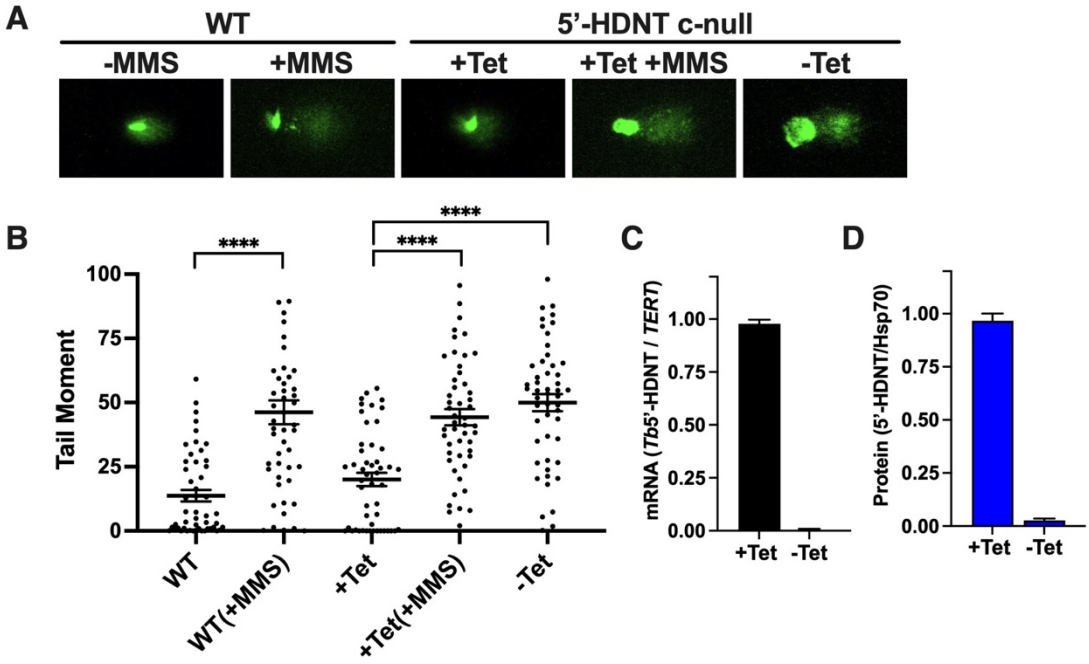
A
WT
5'-HDNT c-null
-MMS
+MMS
+Tet
+Tet +MMS
-Tet
B
Tail Moment
100
75
50
25
0
****
****
****
WT
WT(+MMS)
+Tet
+Tet(+MMS)
-Tet
C
mRNA (Tb5'-HDNT / TERT)
1.00
0.75
0.50
0.25
0.00
+Tet
-Tet
D
Protein (5'-HDNT/Hsp70)
1.00
0.75
0.50
0.25
0.00
+Tet
-Tet

Fig 10

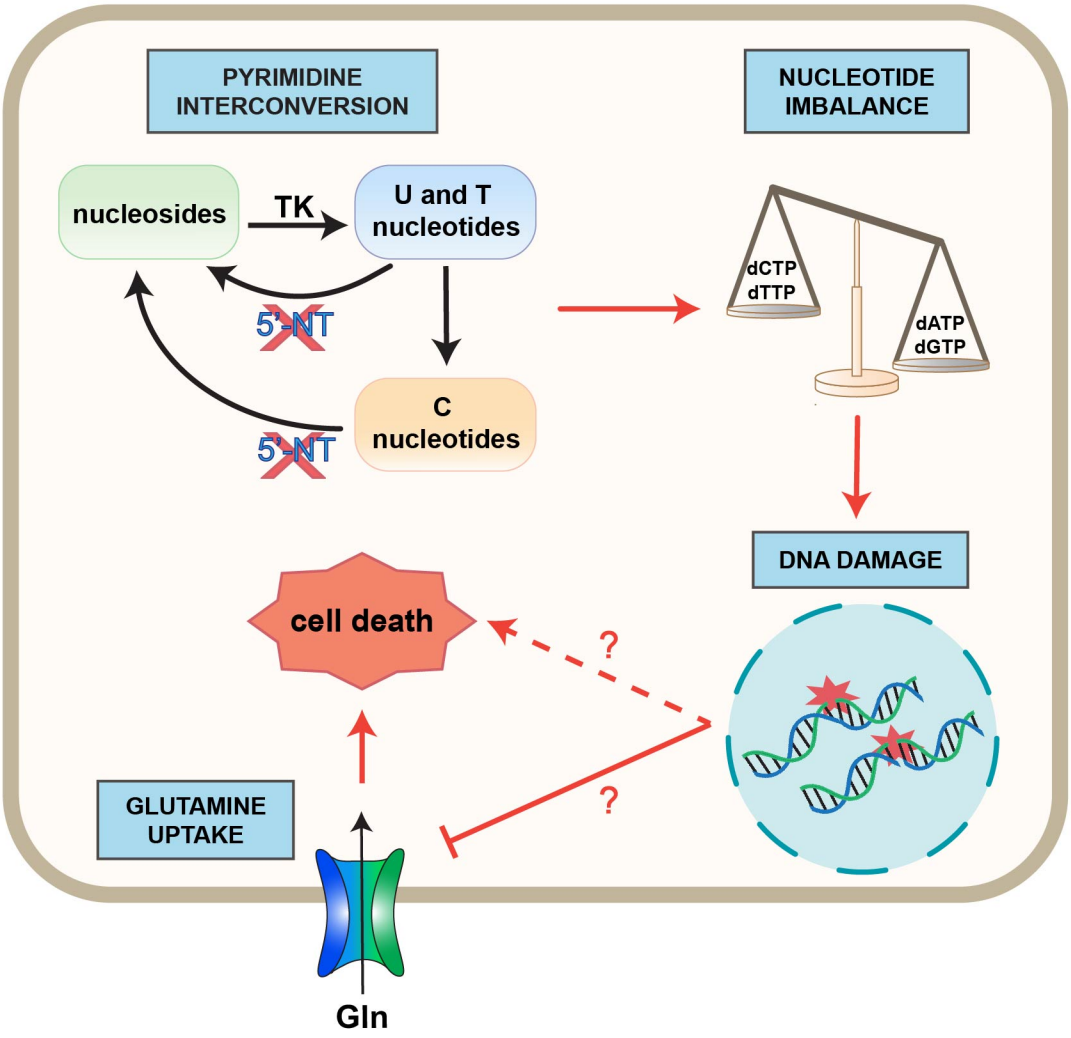
PYRIMIDINE INTERCONVERSION
NUCLEOTIDE IMBALANCE
nucleosides
TK
U and T nucleotides
5'-NT
C nucleotides
5'-NT
dCTP
dTTP
dATP
dGTP
DNA DAMAGE
cell death
?
?
GLUTAMINE UPTAKE
Gln